International Journal of Pressure Vessels and Piping 216 (2025) 105518

Contents lists available at ScienceDirect

International Journal of Pressure Vessels and Piping

journal homepage: www.elsevier.com/locate/ijpvp

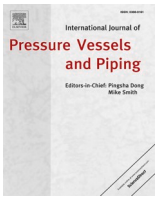

Residual stress analysis in robotically welded plates using phased array ultrasonics with validation through neutron diffraction and hole-drilling methods

Brandon Mills [a,*], Joseph Walker [a], Yashar Javadi [a,b], Charles N. MacLeod [a], Houman Alipooramirabad [c,d], Mark Reid [d], Anna Paradowska [d]

[a] Centre for Ultrasonic Engineering (CUE), Department of Electronic & Electrical Engineering (EEE), University of Strathclyde, Glasgow, G1 1XQ, UK
[b] Department of Design, Manufacturing & Engineering Management (DMEM), University of Strathclyde, Glasgow, G1 1XQ, UK
[c] College of Engineering, Birmingham City University, Millennium Point, Birmingham, B5 5JU, UK
[d] Australian Nuclear Science and Technology Organisation (ANSTO), Lucas Heights, NSW, 2234, Australia

ARTICLE INFO

Keywords:
RS measurement
Phased array ultrasonic testing
Robotic welding
Ultrasonic simulation
Neutron diffraction (ND)
Incremental hole drilling (IHD)

ABSTRACT

This paper explores Residual Stress (RS) measurement in two robotically welded, S275 plates using Phased Array Ultrasonics for Residual Stress Measurement (PAURS) and Neutron Diffraction (ND), with the Incremental Hole Drilling (IHD) method employed for validation. Pogo ultrasonic simulation was used to model the Longitudinal Critically Refracted (LCR) wave and design the ultrasonic setup. Ultrasonic arrays operating at 5 MHz (8 elements) measured RS at a depth of ~1.25 mm. Results show qualitative agreement among PAURS, ND, and IHD, with RS symmetrically distributed on both sides of the plates, validating the effectiveness of phased array probes for qualitative measurement. However, discrepancies in precise numerical values were observed across methods. As PAURS is a novel technique for welded samples, the paper highlights areas for improvement to enhance its quantitative measurement capabilities.

1. Introduction

The focus of this paper is to evaluate the effectiveness of phased array ultrasonic probes used for Residual Stress (RS) detection and measurement. These stresses exist within a material in the absence of external loads or thermal gradients. Welding leads to significant RS development [1], and they can greatly shorten the operative life or lead to unexpected failure [2]. Thus, it is essential to detect and measure these stresses. This can be performed semi-destructively (Hole Drilling [3]), destructively (contour method [4]) or non-destructively (X-ray diffraction [5], Neutron Diffraction [6], ultrasonics [7]). This paper will focus on ultrasonic, Neutron Diffraction (ND), and Incremental Hole Drilling (IHD) methods. IHD was employed as it is standardised by ASTM E837-20 [8], and is often used in RS investigations as a form of verification [9]. It utilises a strain gauge rosette to measure strains released by the incremental drilling of a small hole.

ND utilises a beam of electrons that are diffracted by the microstructure of the material under test [10]. The beam produces an interference pattern, which allows the lattice constant of the material to be accurately obtained, and from this a stress field [11]. The main advantages of this method are the penetration depth and strain resolution. The ND scan is configurable and can give results at depths of up to 50 mm, though the depth resolution is limited to around 1 mm [12]. Additionally, the strains within a sample can be identified to a resolution of 10^{-4} [11]. The main limitation of this method is its cost, as a cyclotron is required to produce the neutron beam used to generate the diffraction pattern. This requirement necessitates the use of specialised laboratories [13], which often have waiting lists, lead times, and associated costs due to high demand. As a result, its application in industry is limited. However, studies like this paper, where multiple methods are used and ND is employed to verify Phased Array Ultrasonics for Residual Stress Measurement (PAURS), which is more accessible to industry, can help improve and refine methods like PAURS, making them more suitable for industrial use in the future [14].

RS measurement using the phased array ultrasonics method in this paper relies on two key factors: the concept of Acoustoelasticity and the Longitudinal Critical Refraction (LCR) technique. The former is the principle that the speed of sound in a given material is intrinsically

* Corresponding author.
E-mail address: brandon.mills@strath.ac.uk (B. Mills).

https://doi.org/10.1016/j.ijpvp.2025.105518
Received 6 January 2025; Received in revised form 12 March 2025; Accepted 24 March 2025
Available online 25 March 2025

affected by the stress the material is under [15]. Unlike other material constants such as Young's modulus or thermal capacity, this value is not included on data sheets, and so must be obtained experimentally. Current standard practice for ultrasonic RS measurement is the usage of the LCR technique [16–18]. This involves inducing a wave parallel to the surface by angling a transmitting receiver at the critical angle, given by Snell's law, that is then picked up by two receiving transmitters at the same angle. Currently, limited research has been performed into the utilisation of this technique using phased array probes instead of single element probes. Javadi et al. [19] have demonstrated that the multiple elements will allow for a more robust stress value in less time, due to the ability to average the results across up to 128 elements in one scan, as opposed to the two of the current single element method. Walker et al. [20] have also demonstrated the importance of verification through different techniques when ultrasonically measuring RS, due to the advantages and disadvantages each method offers. They used the contour method to verify phased array ultrasonics and demonstrated good qualitative agreement between the two methods on titanium WAAM samples. Similarly, IHD and ND are used for verification in this paper. IHD is employed to obtain a robust value for the centre of the sample, while ND is used to obtain RS values at different thicknesses through the material, as the ultrasonic penetration depth is limited by the material's sound velocity and probe frequency [21].

Additionally, in this paper, Pogo simulation [22] is used to great effect in determining preliminary values for experimental equipment, such as the required angle for the wedges to induce the LCR wave.

2. Theoretical background

2.1. Theory of acoustoelasticity

The principle of ultrasonic stress measurement is based on the concept of Acoustoelasticity, which states that a material's stress affects the speed of sound within it. To calculate this mathematically, second- and third-order elastic constants are required. An initial formula is provided by Abiza et al. [23]:

$$L = -\frac{2\lambda(\lambda+2\mu)+\lambda A+2(\lambda-\mu)B-2\mu C}{\lambda+\mu} \tag{1}$$

Where L is the acoustoelastic constant, λ and μ are the second order Lamé constants given by Equations (2) and (3), and A, B, and C are the third order Landau constants, given by Landau and Lifshitz [24].

$$\lambda = \frac{E\nu}{(1+\nu)(1-2\nu)} \tag{2}$$

$$\mu = \frac{E}{2(1+\nu)} \tag{3}$$

A, B, and C are equivalent to the Murnaghan third order elastic constants, such that

$$A = n, B = m - \frac{n}{2}, C = l - m - \frac{n}{2}$$

This allows for Equation (1) to be rearranged, giving:

$$L = -\frac{2\lambda(\lambda+2\mu)+\lambda n+2(\lambda-\mu)\left(m-\frac{n}{2}\right)-2\mu\left(l-m-\frac{n}{2}\right)}{\lambda+\mu} \tag{4}$$

In this paper, the acoustoelastic constant was obtained experimentally through tensile testing, utilising the technique demonstrated by Mohammadi et al. [25]. Although L is experimentally measured, Equations 1-4 emphasise the inherent nonlinearity in the Acoustoelasticity theory. The second- and third-order elastic constants, which contribute to this nonlinearity, are merged into L. While this simplification may introduce some error, the PAURS approach will accurately determine L by generating a large dataset to address the challenge of applying a linear equation to a nonlinear relationship.

2.2. Ultrasonic stress measurement

The velocity of the LCR wave is the most affected by changes in material strain, and is induced parallel to the surface of the sample, by application of Snell's law:

$$\frac{v_w}{v_m} = \frac{\sin\theta_w}{\sin\theta_c} \tag{5}$$

Where v_m and v_w are the sound velocities in the material under inspection and the wedge respectively, and θ_w and θ_c the angle in the wedge and the critical angle respectively. For LCR to properly occur, θ_c must be 90°, which allows Equation (5) to be rearranged to find the required wedge angle:

$$\theta_w = \sin^{-1}\left(\frac{v_w}{v_m}\right) \tag{6}$$

In this study, the sound velocity in wedge was found to be 2730 ms^{-1} and, in the steel, it was 5790 ms^{-1}, giving the first critical angle to be calculated 28.1° based on Equation (6).

The acoustoelastic constant was derived utilising a calibration procedure, where a sample of the material under test was placed into a tensile testing machine, and the time of flight measured. This was used to obtain the final stress in the ultrasonic study, using Equation (7), which is commonly used for RS calculations [26]:

$$\Delta\sigma = -\frac{E\cdot dt}{L\cdot t_0} \tag{7}$$

Here, E is the material's Young's Modulus, L the acoustoelastic constant, t_0 the time of flight under no stress, and dt the difference between the time of flight in the stressed zone of the material and that of the stress-free zone.

It is important to note that Equation (7) must be altered when using phased array probes rather than single element transducers. Taking into account the multiple acoustic paths, the equation becomes:

$$\Delta\sigma = \frac{\sum_{i=1}^{n} -\frac{E\cdot dt_i}{L\cdot t_0}}{n} \tag{8}$$

Where n is the number of ultrasonic elements within the transducer (8 in this study), and dt_i is the ith acoustic path time of flight. Further, when using the Full Matrix Capture (FMC) technique, this equation transforms further, becoming:

$$\Delta\sigma = \frac{\sum_{i=1}^{n}\sum_{j=1}^{n} -\frac{E\cdot dt_{i,j}}{L\cdot t_0}}{n^2} \tag{9}$$

Where $dt_{i,j}$ is the time of flight from the ith transmitter to the jth receiver.

2.3. Neutron diffraction

The ND method is a non-destructive and deep penetration scanning technique that enables the generation of three-dimensional strain maps within engineering components. The neutron beam is deflected by the material lattice according to Bragg's law:

$$n\lambda = 2dsin\theta \tag{10}$$

Where n is the diffraction order, λ thse wavelength of the neutron beam, d the lattice grating constant, and θ the glancing angle of the beam. This will create a diffraction pattern, that can then be used for RS measurement

The lattice strain, ε, is then calculated through measuring the stressed, (d_{hkl}), and stress-free, ($d_{hkl,0}$), inter-planer spacing as given in

Equation (11).

$$\varepsilon_{hkl} = \frac{d_{hkl} - d_{hkl,0}}{d_{hkl,0}} \tag{11}$$

ND can have as high a strain accuracy as ($\pm 50 \times 10^{-6}$) and spatial resolution greater than 0.1 mm [27], and utilises neutrons generated through fission and then moderated by heavy water to lower their energy levels to the thermal range. This allows neutron beams with a consistent wavelength (from a single crystal monochromator) to interact with the sample's inter-planar spacing to produce a scattering angle [28].

2.4. Incremental hole drilling

Incremental Hole Drilling (IHD) is a semi-destructive form of testing. As it is standardised by ASTM E837-20 [8], it is often used in laboratories for validation of novel stress detection methods. This method is carried out by drilling a small hole at the area of interest and measuring the strain relief using a strain gauge rosette, allowing for the production of depth-resolved stress profiles. The relieved strain is given by the equation:

$\varepsilon_r = A(\sigma_{\max} + \sigma_{min}) + B(\sigma_{max} - \sigma_{min})cos\ 2\ \beta$ (12) ere ε_r is the relaxed strain, A and B the calibration constants from the strain gauge, material properties, and hole geometries, β the angle of measurement of strain from the principal direction, and σ_{max} and σ_{min} the maximum and minimum stresses. The equations for the calibration constants are given below:

$$A = \frac{-a(1+\nu)}{2E} \tag{13}$$

$$B = -\frac{b}{2E} \tag{14}$$

Where a and b are dimensionless quantities that vary with hole depth, E is the Young's Modulus of the material, and ν is the material's Poisson's ratio.

However, equation (12)only refers to measuring uniform RS using the IHD method. In the case where the RS distribution is non-uniform with depth, then a different formula is required:

$$\varepsilon_j = \sum_{k=1}^{n} A_{jk}\sigma_k \tag{15}$$

Where ε_j is the measured strain relief at the *j-th* depth increment, σ_k is the RS at the *k-th* depth increment, A_{ij} is the calibration constant that relates to the stress relief at depth j to the stress at depth k and n is the total number of depth increments.

3. Methodology

3.1. Overview of manufacturing, simulation and residual stress measurement

This research was conducted as a collaboration between several institutions, and an overview of the process is provided in Fig. 1 as detailed here.

A) Two identical samples were robotically manufactured at the University of Strathclyde (Glasgow, UK), with one remaining in the UK and the other shipped to Australia for neutron diffraction (ND) at ANSTO (Lucas Heights, Australia).
B) Sample #1 was first sent to Stresscraft (Loughborough, UK) for IHD. Although the IHD process is semi-destructive and required machining of the weld cap to prepare it for drilling, the sample remained suitable for ultrasonic testing, which also requires a near-flat surface. It is worth noting that the machining process used during IHD has an influence, and the residual stress state near the surface can be affected by several hundred microns. While this could potentially induce error in both ultrasonic and IHD measurements, it is believed that its effect is minimised in this paper for the following reasons: (I) the IHD is primarily used for the verification of the ultrasonic results, so this error remains consistent in both measurements, and (II) while the machining can affect the residual stress for several hundred microns, the ultrasonic measurement was conducted at a greater depth (~1.2 mm).
C) Sample #1 was subsequently returned to the University of Strathclyde (Glasgow, UK) for RS measurements using the phased array ultrasonic method.

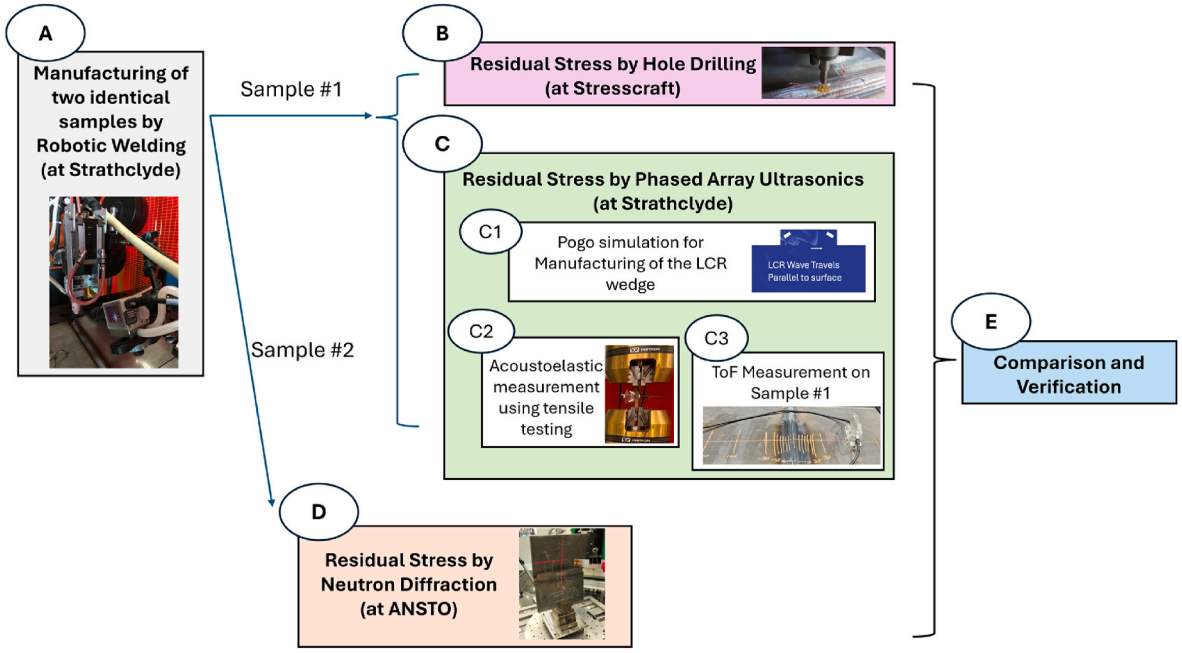

Fig. 1. Overview of experimental procedures and institutions involved.

C1 At Strathclyde, initial ultrasonic simulations were conducted prior to wedge manufacturing to optimise the angle for generating LCR waves. Following wedge manufacture, the penetration depth of the LCR wave was calculated and experimentally validated.
C2 The acoustoelastic constant was then measured through tensile testing.
C3 Finally, Time of Flight measurements were carried out on Sample #1 to complete the phased array ultrasonic investigations.

D) Sample #2 was sent to ANSTO (Lucas Heights, Australia) for RS measurements using neutron diffraction.
E) After all inspections were completed, the phased array ultrasonic, ND, and IHD results were collated for comparison and verification.

A schematic of the techniques used and their relative scan positions on the weld is presented in Fig. 2. This gives an overview of the relative depths and areas where these methodologies were applied.

3.2. Sample manufacturing

Two identical samples were manufactured robotically from S275 structural steel plates, with a length of 300 mm and a thickness of 15 mm. The weld was deposited over 21 passes, deposited in 7 layers within a 90° V groove. This was performed using Tungsten Inert Gas (TIG). An Automatic Voltage Correction (AVC) system was implemented to keep the welding voltage constant throughout the process, utilising real-time communication between the robot controller and the welding setup offered by the KUKA Robotic Sensor Interface (RSI) [29]. The welding parameters can be found in Table 1, the pass layout in Fig. 3, and the manufacturing setup in Fig. 4. Throughout the welding process, the sample was tightly clamped to the welding table, with the aim of increasing the final RS present in the sample by preventing any relief from plastic deformation. From the manufacturer, the Young's Modulus of the sample is 205 GPa, and the Poisson's Ratio 0.295.

The reason for using robotic welding, apart from achieving higher quality welds, was to produce two identical samples, as shown in Fig. 4, due to the repeatability provided by the robot. One sample was kept for PAURS at the University of Strathclyde (Glasgow, UK), along with IHD experiments at Stresscraft Ltd (Loughborough, UK), while the other was sent to ANSTO (Lucas Heights, Australia) for ND inspection (see Fig. 14).

3.3. Incremental hole drilling

The IHD process was carried out according to ASTM E837 – 20 [8] in three positions on the sample. The first point was taken 20 mm below the centre of the weld, with respect to the length and width. The further two points were taken 20 mm and 40 mm above the initial point to increase the overall measurement accuracy, with the 20 mm separation implemented to avoid the surface preparation affecting the measurements at other points. An example of this setup from the initial point is shown in Fig. 5.

This procedure involves incrementally drilling a hole at each point while a strain gauge bonded to the sample surface measures the strain relaxation after each increment. The strains can be related to the amount of RS released with the minute deformations the IHD causes. Following the surface preparation, the strain gauges were bonded such that element 1 of each gauge was oriented in the weld direction, and element 3 was oriented perpendicular to the weld. The holes were drilled in 16 increments, set at 4 of 32 μm, 4 of 64 μm, and 8 of 128 μm for a total hole depth of just over 1.4 mm and stress data to a depth of 1.02 mm. During each drilling increment, the strain gauges recorded real-time strain data, reflecting localised stress release as material was progressively removed. These strain values were then analysed using standardised calibration coefficients and mathematical models outlined in ASTM E837 to calculate the RS profile. The hole diameter was 2 mm, and the gauge type used was 062RE. The maximum evaluation depth for IHD is limited to approximately half of the hole diameter, as reliable results are difficult to obtain beyond this depth, where high scattering is typically observed in stress measurements [30]. This limitation is intrinsic to the technique, however it did not affect the ultrasonic method, where 5 MHz transducers were employed to approximately match the maximum stress data depth for sake of comparison (see Sec. 3.4.2). Aligning the IHD and LCR measurement depths facilitated direct comparisons between mechanical and ultrasonic stress measurements, enhancing the validation and reliability of the overall study results.

3.4. Phased array ultrasonics for residual stress measurement (PAURS)

3.4.1. Ultrasonic simulations

Pogo is a software developed for explicit time-domain finite element simulations of elastodynamic problems on GPUs using Nvidia's CUDA [31]. It optimises memory arrangement through efficient mesh partitioning, utilising both a "greedy" and a more advanced "aligned" partitioner. When applied to models in non-destructive testing, vibrations, and geophysics; Pogo achieves near-maximum GPU memory bandwidth - demonstrating a speed two orders of magnitude faster than the CPU-based Abaqus software while maintaining comparable accuracy.

Pogo has many ultrasonic simulation applications, such as guided waves [31] determination of the backscattering coefficient [32], and Rayleigh wave attenuation [33]. It has not yet been used for simulation of the LCR wave. In this paper, Pogo was used for the simulation of the LCR wave propagation to optimise the wedge angle required for the follow-on PAURS process. A model was created of the arrays, wedges,

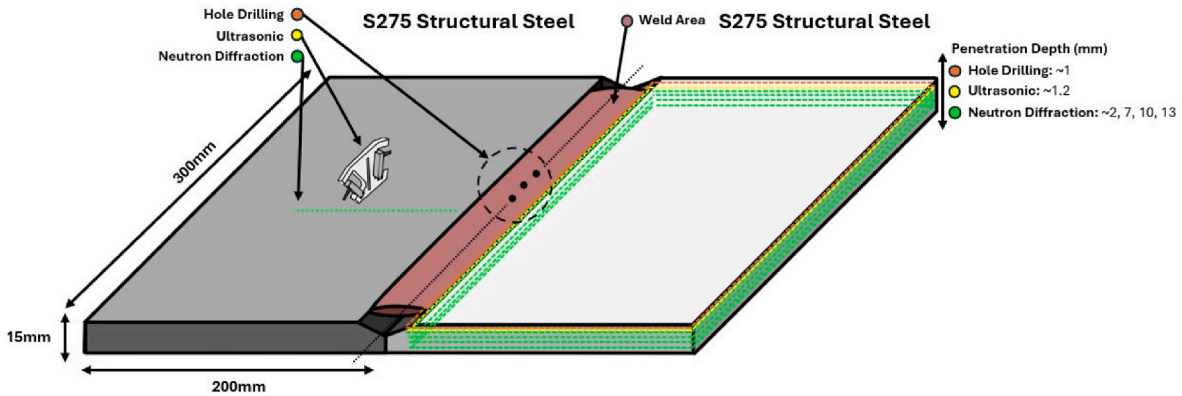

Fig. 2. Schematic overview of RS investigations performed on samples.

Table 1
Welding parameters.

	AVC Set Voltage (V)	Current (A)	Travel Speed (mm/min)	Weaving Amplitude (mm)	Weaving Frequency (Hz)	Inter-Pass Temperature (°C)
Pass 1 (root pass)	12	120	50	2	0.3	80–100
Pass 2 (hot pass)	13.5	220	100	4	0.6	80–100
Passes 3–16 (filling passes)	13.5	210	120	3	0.55	80–100
Pass 17–21 (capping passes)	13.5	240	100	4	0.6	80–100

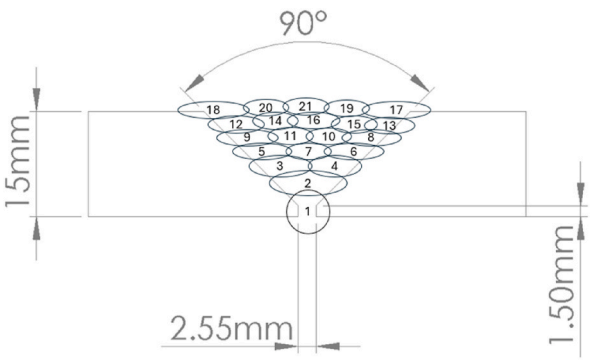

Fig. 3. Weld layout diagram.

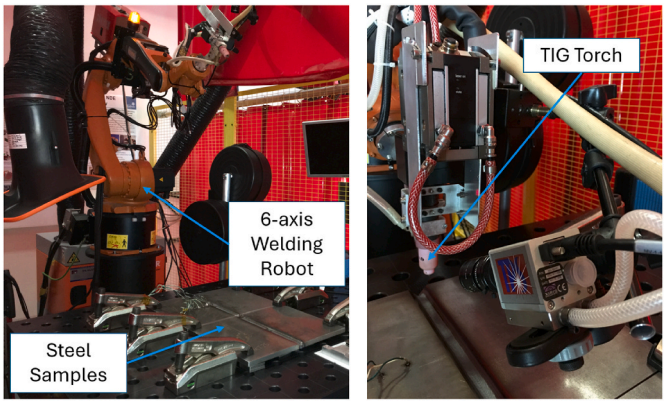

Fig. 4. Setup for robotic manufacture of weld samples.

and sample, and simulations run to identify the ideal angle to propagate LCR wave, and the expected depth of the LCR wave within the sample (Fig. 6).

After optimizing the wedge angle based on the wedge material and steel sample in the Pogo model, the LCR wave was successfully generated, as demonstrated in Fig. 7. Snapshots from the simulation illustrate the propagation of ultrasonic waves triggered by the transmitter array elements. These waves travel through the wedge, refract at the boundary with the sample, and propagate parallel to the surface within the steel, confirming the characteristic behaviour of LCR waves. The waves then redirect towards the receiver at the intersection of the LCR path and a line from each receiver element, demonstrating accurate modelling.

LCR waves can be classified as longitudinal surface creeping waves (LSCW) or subsurface longitudinal waves (SSLW). While LSCWs decay rapidly within a few centimetres, SSLWs travel long distances, up to 300 mm, at near-bulk longitudinal wave speeds, retaining strong amplitudes [34]. The longitudinal wave beam profile confirms the generation of LCR waves at the steel plate surface, with the principal energy lobe refracting at 84°, aligning with the characteristics described by Bray and Tang [35]. These waves are more sensitive to stress and less affected by localised material texture changes compared to shear waves, and thus are often used for RS measurement. Our Pogo model accurately replicates these LCR wave behaviours, which have been overlooked in recent publications despite their significance since Bray et al.'s findings in 2000 [34]. This study represents the first successful attempt to simulate LCR waves using finite element modelling, paving the way for further advancements in simulating RS measurements via ultrasonic methods. Additionally, the visualisation of all 64 acoustic paths generated by the two 8-element arrays demonstrates potential for Time of Flight measurements and the further development of PAURS procedure.

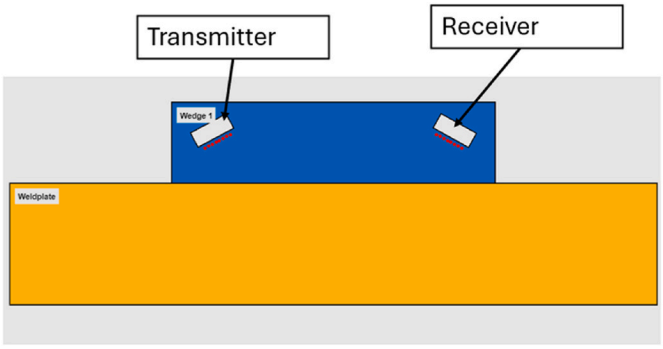

Fig. 6. Model for ultrasonic simulation to determine ideal wedge angle.

Fig. 5. Example of Incremental Hole Drilling setup at first position tested. (a) Point Marking. (b) Surface Preparation (c) Incremental Hole Drilling.

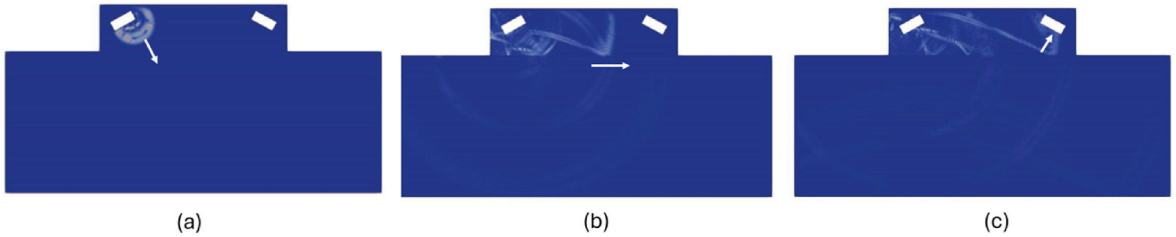

Fig. 7. Progression of the LCR wave across the simulated sample (a) The pulse is initiated. (b) The pulse propagates across the sample. (c) The pulse encounters the receiving transducer.

The Pogo simulation results validated the calculated angle to induce the LCR wave. Following this, an acrylic wedge with angles of 28.1° was laser cut for use in the following experiments (Fig. 8). The slit in the wedge was purposefully designed in order to compromise between wedge robustness for future robotic testing and the avoidance of cross-talk between the probes. As a result, the slit is not surface breaking, but protrudes low enough such that any potential crosstalk would be minimised and easily calibrated out.

Additionally, within this study the Full Matrix Capture (FMC) technique was used to maximise the amount of data extracted. Within this study distinction between FMC and linear scans are made, where linear scans consist of matched transmit – receive element pairs (T1-R1 for example) and FMC scans include linear scans, but additionally send and receive on each element (T8 – R4 for example). A visualisation of this can be seen in Fig. 9.

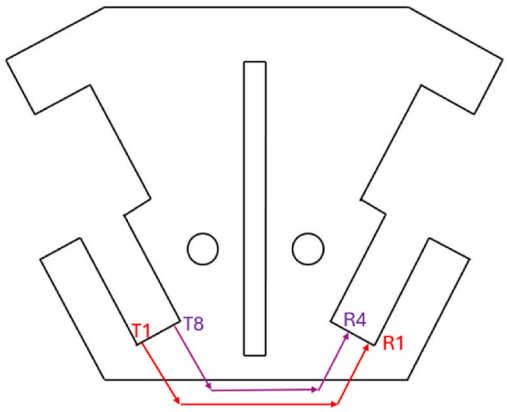

Fig. 9. An Example of a linear acoustic path (Red) and an acoustic path from an FMC scan (Purple).

3.4.2. *Penetration depth study*

One advantage of RS measurement using the ultrasonic method is its ability to measure stress at varying depths by adjusting the transmitter and receiver frequencies [9]. However, in PAURS measurements, penetration depth introduces additional complexity compared to single-element studies. The vertical stacking of array elements can result in slight variations in penetration depth for each element, requiring careful consideration in analysis. Using the equation from Hwang et al. [16]:

$$D = c \times f^{-0.96} \tag{16}$$

Where D is the penetration depth, c the sound velocity within the material, and f the frequency of the ultrasonic probe, an expected value of roughly 1.2 mm was calculated. To verify this calculation, an experiment was designed to measure the penetration depth of the LCR wave generated by the arrays used in this study. A plate of similar material was used to determine the ultimate penetration depth. Notches ranging from 0.5 mm to 7.75 mm in depth were introduced, increasing in 0.25 mm increments, as shown in Fig. 10. The ultrasonic wedge was moved from Point A, where the notch depth was 0.5 mm, to Point B, where the notch depth was 4 mm. Along this path, notches of different depths were encountered, increasing in increments of 0.25 mm, up to 4 mm at Point B.

An example of the A-scan generated by element 1 of the transmitter and received by element 1 of the receiver (64 A-scans were recorded in total using 8-element arrays) for selected notches is shown in Fig. 8. The A-scan at Point A (Fig. 11a) clearly exhibits the LCR wave. However, the amplitude of the LCR wave decreases for a notch with a depth of 1.25 mm (Fig. 11b), becomes even lower for a depth of 1.5 mm (Fig. 11c), and is nearly undetectable for a notch with a depth of 1.75 mm (Fig. 11d).

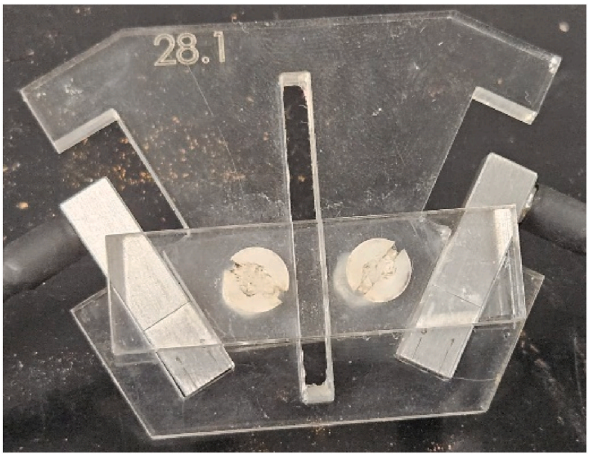

Fig. 8. Manufactured wedge with arrays, for fit test. An acrylic bar was added on either side to keep the probes in place.

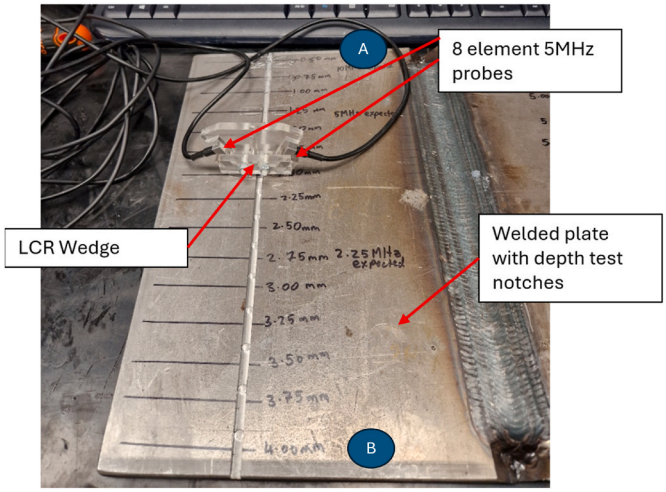

Fig. 10. Experimental setup for penetration depth study. The indications marked are the slot depths.

These results indicate that the maximum depth at which the 5 MHz array can reliably detect the LCR wave is approximately 1.5 mm. In this study, a penetration depth of 1.25 ± 0.25 mm was considered optimal.

3.4.3. Acoustoelastic constant calibration

A representative dumbbell-shaped sample of material was used in a tensile testing machine to determine the acoustoelastic constant (Fig. 12). The experimental setup involved securing the LCR wedge assembly to the tensile test sample and measuring the ultrasonic time of flight at various load points. These time-of-flight measurements, combined with the stress data obtained from the tensile testing machine and the material's known constants, were used to rearrange Equation (9) such that by fitting a line to the experimental data, the acoustoelastic constant could be extracted from the slope.

Two separate tests were conducted using this setup. The first test involved loading and unloading the sample from 0 kN to 48 kN in increments of 3 kN. The second test provided a more detailed analysis by loading and unloading the sample from 0 kN to 57 kN in smaller steps of 1 kN. This approach ensures that errors caused by possible sliding of the wedge over the sample (noting that the sample elongates during tensile testing) are minimised, as the average of hundreds of data points will be considered. For example, in this test, we collected 16 data points for loading in Test #1 and another 16 data points for unloading. Each data point includes FMC data acquisition, which involves 8x8 or 64 acoustic paths. This results in 64x32 data points. Similarly, for Test #2, 57 data points were collected for loading and 57 for unloading, yielding 114x64 data points. Altogether, this provides 9344 data points compared to equivalent RS measurements using a single-element probe [36]. During each test, the tensile testing machine paused for 10 s at each load increment to allow ultrasonic A-scan data acquisition.

A MATLAB algorithm was employed to process the collected data. The algorithm extracted the time of flight of the LCR wave using user-defined time-gating techniques. From the extracted time-of-flight data, the acoustoelastic constant was calculated on a per-element basis. The results were then averaged to derive a representative value of the acoustoelastic constant for the material. This constant was subsequently used in the broader PAURS study of the welded plate.

3.4.4. Ultrasonic inspection of welded plate

The ultrasonic inspection of the welded sample was performed by scanning the welded sample, using PAURS system, in 21 discrete points, moving perpendicular to the weld to obtain the longitudinal RS (Fig. 13). The gap between these points was initially large (50 mm) in the parent material, before reducing to 5 mm increments in the Heat Affected Zone (HAZ) as that is where the most variance in RS is expected. Difficulties were encountered in the weld geometry, as most of these areas were not sufficiently smooth to provide a solid connection between the wedge and the sample, but this was accepted as machining of this area would relieve the RS present and would lead to the invalidation of any possible comparison between methods. Therefore, in these

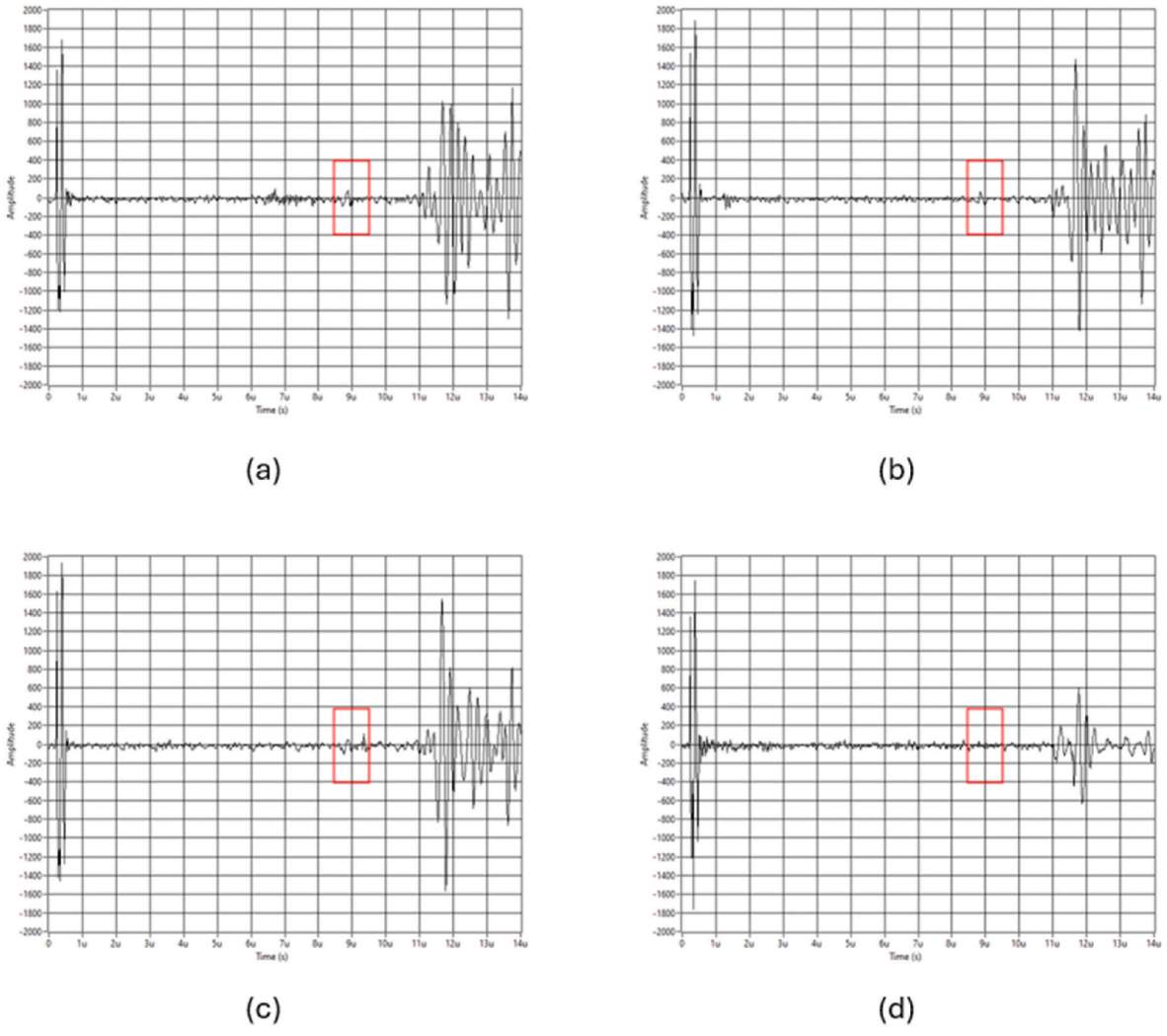

Fig. 11. A-scans at (a) 0.5 mm, (b) 1.25 mm, (c) 1.5 mm, and (d) 1.75 mm depths with LCR wave position highlighted.

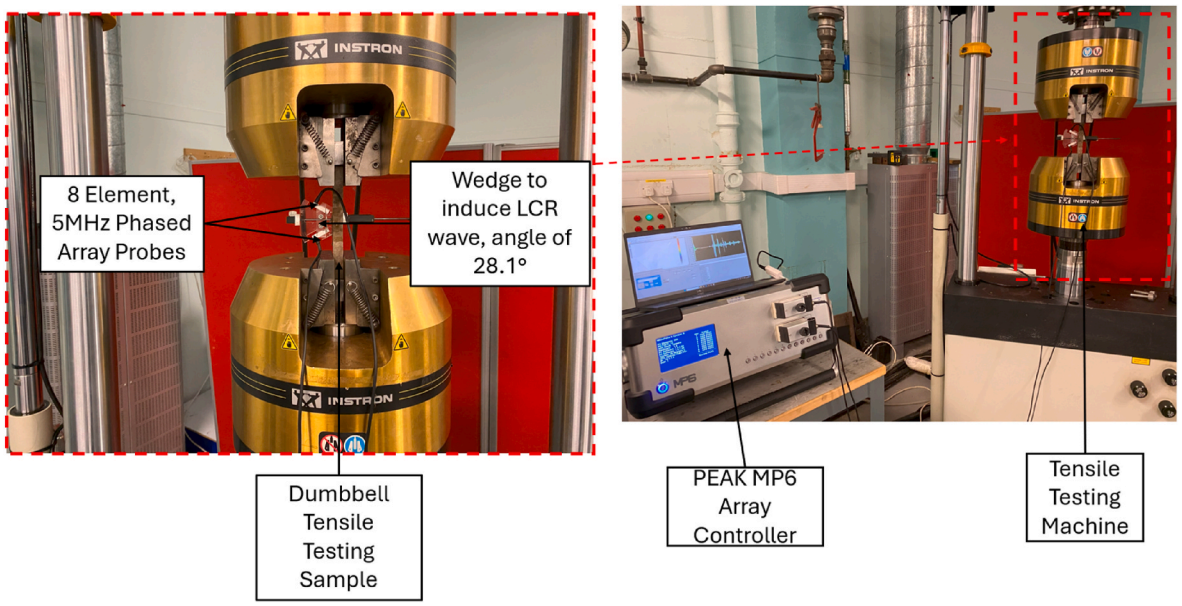

Fig. 12. Acoustoelastic calibration experimental setup.

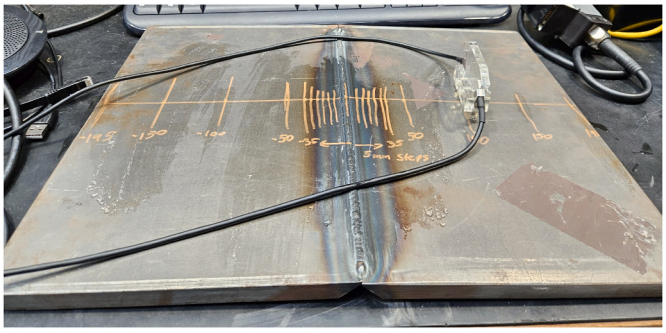

Fig. 13. Ultrasonic testing of sample.

areas (denoted by a grey boundary in the PAURS results section) the comparison sought is purely qualitative.

The 21 scan positions were arrayed in a symmetrical pattern. The FMC technique was additionally used to maximise the data acquired. The A – scans captured were processed using the same MATLAB algorithm as in the previous section, retooled to calculate RS. A schematic of the process can be seen in Fig. 14

The RS was extracted by determining the second zero crossing of the LCR wave, which was located within a user defined window. The overall stress was calculated using Equation (9) and presented relative to the scan position, using the previously determined acoustoelastic constant, the extracted time of flight for stressed and unstressed positions, and relevant material constants.

3.5. Neutron diffraction

The ND technique utilises Bragg's Law to identify changes in atomic lattice spacing resulting from stress within a component, treating the lattice spacing as a gauge for strain. To calculate absolute stress values, the method requires measurements of lattice spacing in an unstressed material sample to establish the stress-free lattice parameter (known as a d0 sample). By measuring the relative shift of the lattice spacing relative to the d0 sample, the RS can be calculated and isolated from any additional material properties that can cause a lattice shift. ND enables bulk stress measurements at depths reaching tens of millimetres, unlike other techniques that measure only a few micrometres. ND measurements for this study were performed on the KOWARI strain diffractometer at the ANSTO facility in Australia (Fig. 15). The depths chosen in this experiment were 2 mm, 7 mm, 10 mm, and 13 mm, to both give a through-thickness stress profile of the sample and provide reference for the ultrasonic measurements across the top and bottom of the sample.

A monochromatic neutron beam with a wavelength of 1.67 Å was used within a gauge volume of $2 \times 2 \times 2$ mm^3 to measure the scattering angle from the α-Fe (211) reflection. RS measurements were performed in three principal directions across the weld at the four different depths.

To obtain stress-free reference samples, Electrical Discharge Machining (EDM) with a 0.2 mm wire diameter was used to extract 5 mm thick slices ($5 \times 80 \times 20$ mm^3) from the weld region at the plate's centre. These samples were taken from locations corresponding to the measured interplanar spacing points (d-spacing) to ensure accurate comparison. The extraction method was designed to achieve complete residual stress relief, following an approach previously applied in studies on HSLA and quenched-and-tempered steel welds [27].

3.6. Comparison and verification

The results from the separate investigations were collated for post processing within MATLAB. This integrated approach allowed for a comprehensive analysis and direct comparison of the different measurement techniques, facilitating a robust assessment of RS within the sample. Those results directly comparable (PAURS scans of the top and bottom of the sample, IHD, and the ND scans at depths of 2 mm and 13 mm) were superimposed on a single graph, which facilitated the comparison of the trends and numerical data. This will be discussed further in the results section. Fig. 16 illustrates the detailed comparison processes, describing the sequence of steps undertaken—from data collection through ND, IHD, and PAURS techniques, to MATLAB-based data processing and final comparative analysis. This figure serves as a roadmap, highlighting the integration of multiple methodologies and emphasizing the thoroughness of the approach in validating RS measurements. Additionally, a standard deviation study was performed, comparing the stress calculated on individual linear and FMC acoustic paths with their respective averages. The study aimed to assess the consistency and reliability of the measurements.

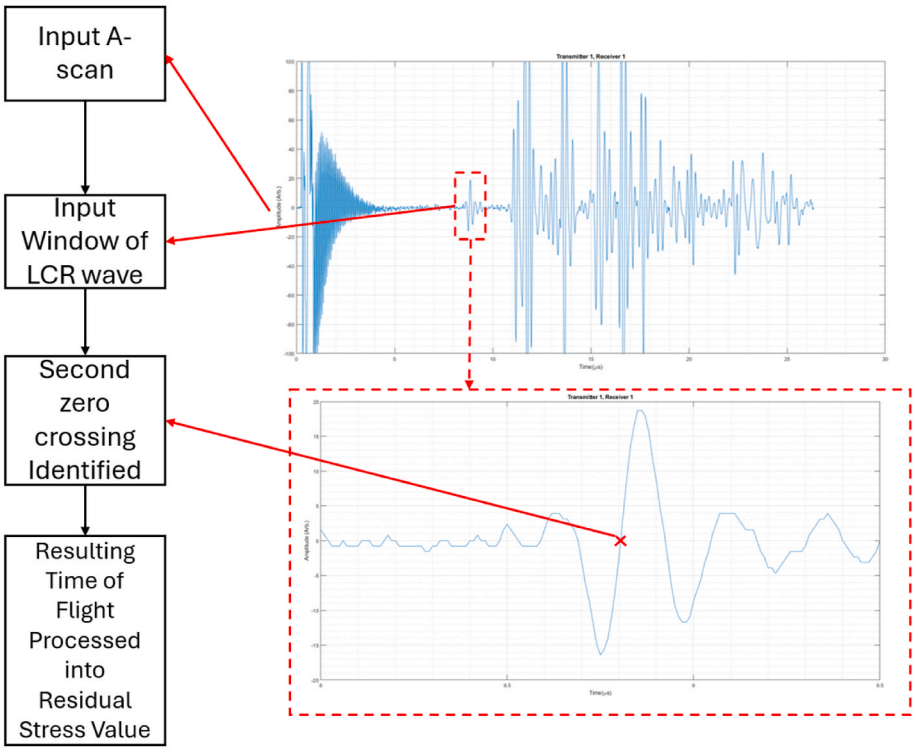

Fig. 14. Flowchart visualisation of RS extraction algorithm.

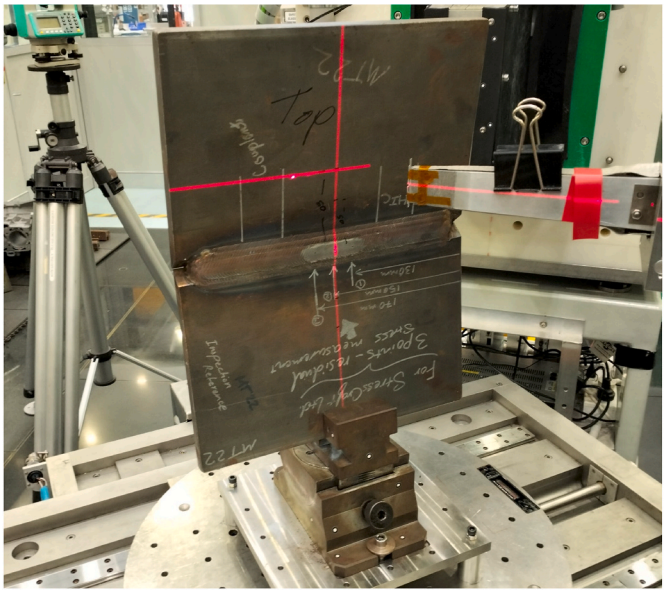

Fig. 15. ND experimental setup.

4. Results and discussion

4.1. Incremental hole drilling

The results of the IHD method are shown in Fig. 17. This method was performed across the depth of the weld itself, focusing specifically on the weld centre rather than spanning the length of the weld plate. Consequently, the IHD results correspond directly to the centre point data obtained from the ND and PAURS scans. Given the inherent uncertainties in the ultrasonic measurements at the weld centre, IHD provides a critical verification tool for validating these results and enhancing confidence in the overall stress assessment.

The IHD technique introduces its own set of uncertainties that must be carefully considered. The accuracy of IHD measurements varies significantly with depth. In the shallowest regions (up to 200 μm), the stress uncertainty is relatively high, reaching approximately ±60 MPa. This high variability is due to several factors, including surface preparation inconsistencies, strain gauge bonding effects, and the difficulty in determining the zero depth accurately. While these issues can all be mitigated experimentally, and there is a clear reproducibility among the three measurement locations, the high stress gradient near the surface suggests that these variations may also reflect the actual residual stress distribution rather than purely measurement artifacts. However, given the inherent sensitivity of IHD in this region, these early results were ultimately excluded from comparative analyses to ensure consistency and minimize uncertainty effects in the final assessment. The uncertainty then decreases to a minimum of ±11 MPa and a maximum of ±25 MPa around a depth of 500 μm. This range represents the most reliable portion of the IHD measurement process, where the effects of surface irregularities and initial material inconsistencies are minimised. Beyond this depth, the uncertainty gradually increases again, reaching a maximum value of approximately ±42 MPa at the final increment (1 mm depth). The increase can be attributed to factors such as cumulative strain gauge errors and potential misalignment during deeper drilling stages. The results within the first 200 μm of the IHD process were excluded from comparative analyses due to the influence of the surface preparation. Focusing on the 200–1000 μm range ensures that only the most relevant data points contribute to the evaluation. This selective approach minimises the impact of early-stage inaccuracies and enhances the overall robustness of the RS assessment.

Alas, the IHD method was not applied to the bottom surface of the weld sample, as it was decided that a robust value for the top of the sample was more desirable than a less robust value for one side and a single data point on the other. As a result, there is no IHD-derived data to verify the ultrasonic measurements at this location. This absence represents a limitation in the comparative analysis, underscoring the importance of comprehensive sampling across all critical regions in

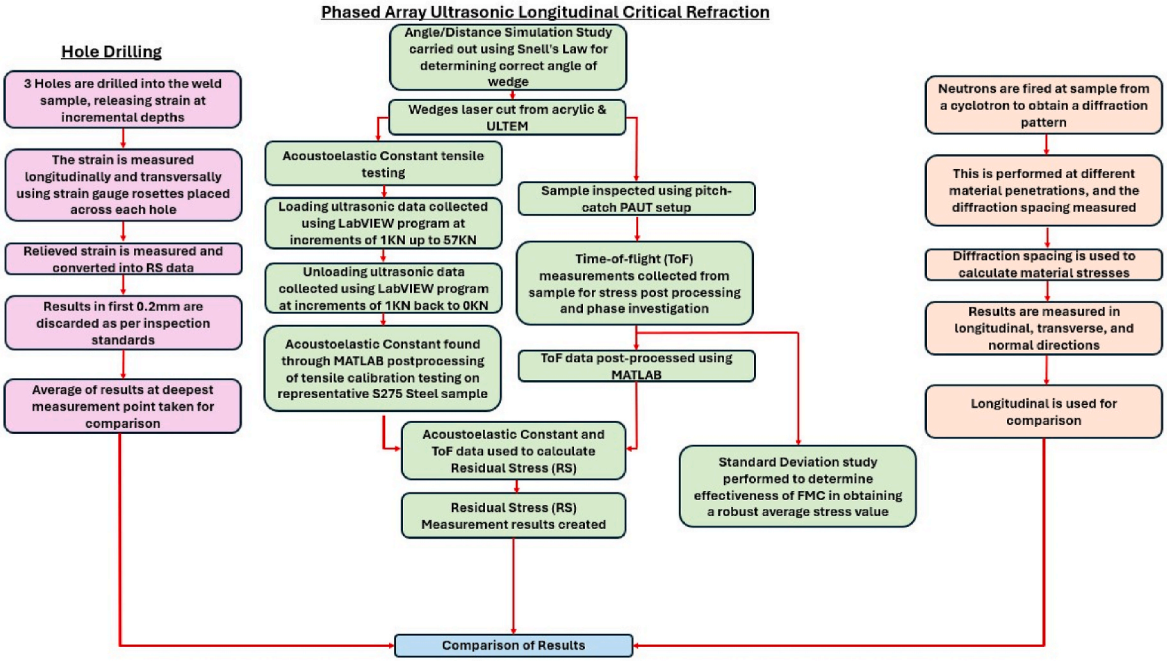

Fig. 16. Overall project workflow, leading into the final result comparison.

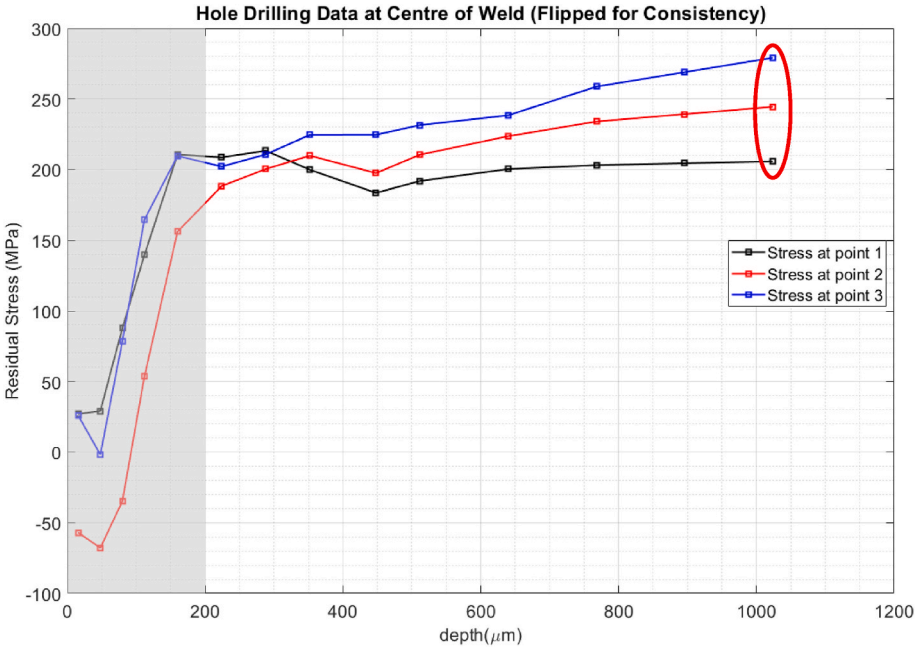

Fig. 17. IHD results, with shaded area up to 200 μm to indicate results that are to be discarded.

future investigations. Overall, the three results at ~1000 μm depth (within the red outline in Fig. 26) were averaged to give a value for comparison of 243 ± 42 MPa.

4.2. Phased array ultrasonics for residual stress measurement (PAURS)

4.2.1. Acoustoelastic calibration

The acoustoelastic constant was extracted by plotting the known stress from the tensile testing machine against the Young's Modulus of the material multiplied by the ratio of the time delta and the initial stress free time (Figs. 18 and 19). By rearranging the fundamental acoustoelastic equation (Equation (7)), a linear relationship was established between the known stress ($\Delta\sigma$) and the ultrasonic time of flight delta ratio. This linear form allowed the acoustoelastic constant (L) to be extracted as the gradient of the resulting best-fit line.

The slope of this line represents the acoustoelastic constant, which quantifies how the ultrasonic wave velocity changes with applied stress. Figs. 18 and 19 illustrate the calibration results, revealing a linear relationship between the known stresses and the normalised ultrasonic time changes. However, the minimal variation observed between the numerous data points across all 8 individual measurement elements posed a challenge in distinguishing subtle differences. The lack of variance could have limited the precision of individual measurements, but by averaging the results, a more reliable and representative line of

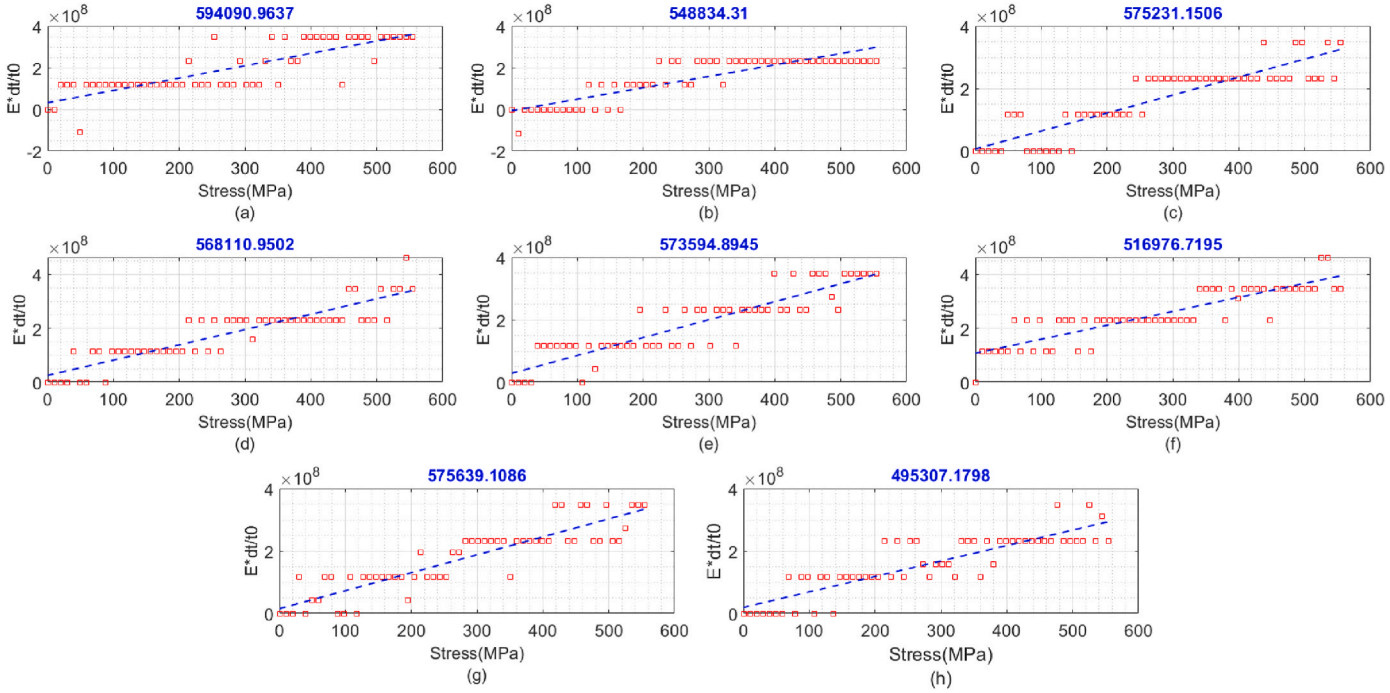

Fig. 18. Element-wise results for the Acoustoelastic Constant during the loading of the sample (a is transmitter 1 to receiver 1, b is transmitter 2 to receiver 2, etc.).

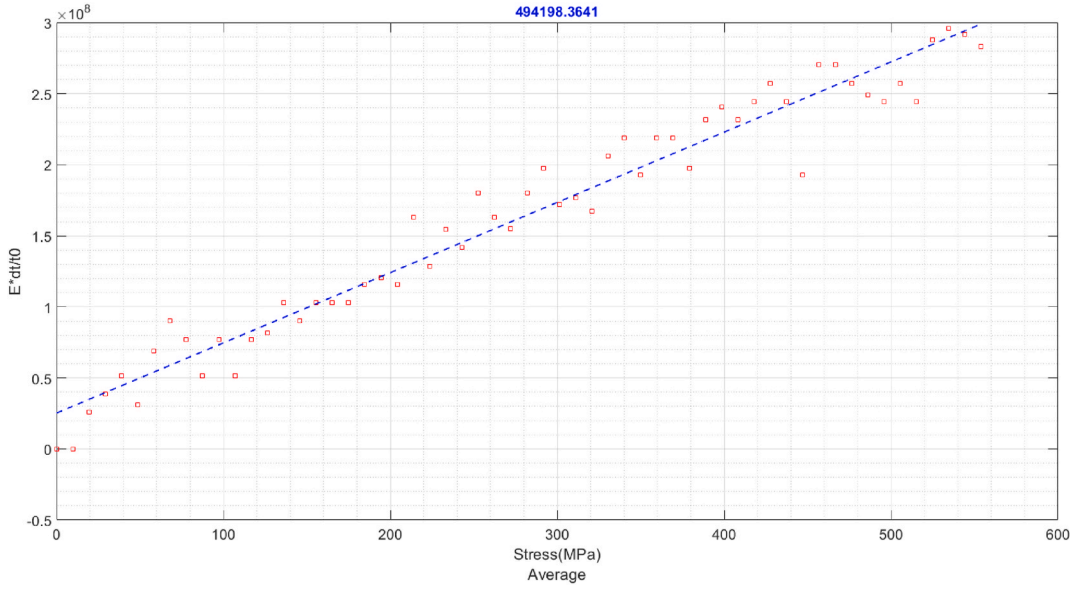

Fig. 19. Average acoustoelastic constant.

best fit was obtained. This approach effectively mitigated the potential impact of uniformity, ensuring the robustness and accuracy of the overall measurement process.

The gradient of the best-fit line, highlighted in blue on each graph, represents the acoustoelastic constants obtained from different measurement elements. The final value used for the weld investigation was determined to be 4.95×10^5. The extracted acoustoelastic constant provides the necessary calibration for interpreting ultrasonic data in the context of RS measurement.

It is worth noting that only the results of one of the four datasets (loading/unloading for Test #1 and Test #2) discussed in Section 3.4.3 are presented here for brevity, while the complete set of four datasets, comprising 9344 data points, was utilised to minimize errors caused by couplant variations and wedge sliding.

4.2.2. *Ultrasonic residual stress investigation*

The ultrasonic inspection of the sample was performed per standard procedures for a single element ultrasonic RS investigation, with the exception of using two phased array probes in pitch catch configuration in place of the three single element probes. During the inspection, the second zero crossing of the LCR wave was recorded for each element and scan position across the top and bottom surfaces of the sample. This specific crossing point was chosen because it provides a consistent and reliable reference for detecting minute changes in the LCR wave travel time, which is directly related to RS within the material. This recorded time of flight data was processed using the previously determined

acoustoelastic constant (derived from the tensile calibration tests). Applying this constant within Equation (9) allowed the calculation of RS at each measured point. These calculations generated a detailed RS map, representing stress distributions at a depth of approximately 1.2 mm into the sample. A selection of individual element results are shown in Figs. 20 and 21:

Following this, the average of all 64 acoustic paths was taken for each scan position, and collated into a final RS distribution (Figs. 22 and 23) across the top and bottom of the sample. A peak stress of approximately 290 MPa was observed on both surfaces, indicating significant RS likely introduced by the welding process. These stresses are critical to assess, as they can influence the mechanical performance and long-term durability of the weld.

Special consideration must be given to the data points within the central region of the weld (between −25 mm and 25 mm on Fig. 22, and –5 mm and 5 mm on Fig. 23). The material geometry within these areas make it difficult to obtain a solid interface between wedge and sample, and any machining to improve this would relieve stresses present and invalidate comparisons. As a result, the measurements in this region exhibit greater uncertainty compared to points farther from the weld centre. This variability underscores the need for cautious interpretation when analysing stresses in highly altered zones. Additionally, in Fig. 22, an RS value of around −50MPa is observed at −200mm, and around 50 MPa at 200 mm. It is understood that this is due to clamping forces during the robotic welding (see Fig. 4). A similar RS behaviour in the parent material was also reported by Javadi et al. [37], who investigated the clamping effect on welding sub-surface residual stress and deformation. Javadi et al. reported 250 MPa RS at the centre of the weld but around 75 MPa in area affected by the clamps (top surface of the plate), within the parent material. However, they observed a much smaller effect at a depth of 6 mm from the top surface, with only 25 MPa. These results align with the observations in this paper, where approximately 50 MPa stress is seen on the top surface (Fig. 22), while the RS in the parent material becomes negligible when measured from the bottom of the sample (Fig. 23).

The standard deviation of RS values along individual acoustic paths was analysed to assess measurement consistency. When considering only the matched transmit-receive pairs—traditional linear paths—the standard deviation was notably high (Figs. 24 and 25). This suggests that relying solely on these linear paths may introduce localised inaccuracies, particularly in complex or heterogeneous materials like welds. The analysis showed that when the full complement of acoustic paths from FMC was used, the standard deviation was lowered by factors of 5–10 (Figs. 26 and 27).

These positions were chosen to give examples from the 3 main metallurgical areas within the weld: the PM, the HAZ, and the weld itself. It can be observed that consistently the PM has a lower average standard deviation across all paths considered than the HAZ and weld areas, and additionally the bottom of the sample exhibits a lower variance than the top, likely due to the welding process having a much more limited effect coupled with lessened impact from the clamping forces present during manufacture.

The significant reduction in deviation between FMC and linear scans demonstrates the FMC method's superior ability to mitigate inconsistencies and noise, leading to a more accurate and reliable RS assessment.

4.3. Neutron diffraction

The ND results provided a comprehensive view of the RS distribution throughout the weld sample. This technique offers valuable insights into the internal stress state, capturing stress profiles at different depths and across multiple directions, essential for a complete stress assessment in welded structures. Three principal stress components were extracted from the ND data (Fig. 28).

1. Longitudinal Stress (Parallel to the weld):

This is the primary stress component along the length of the weld and is typically the most significant due to the thermal expansion and contraction during welding.

2. Transverse Stress (Perpendicular to the weld):

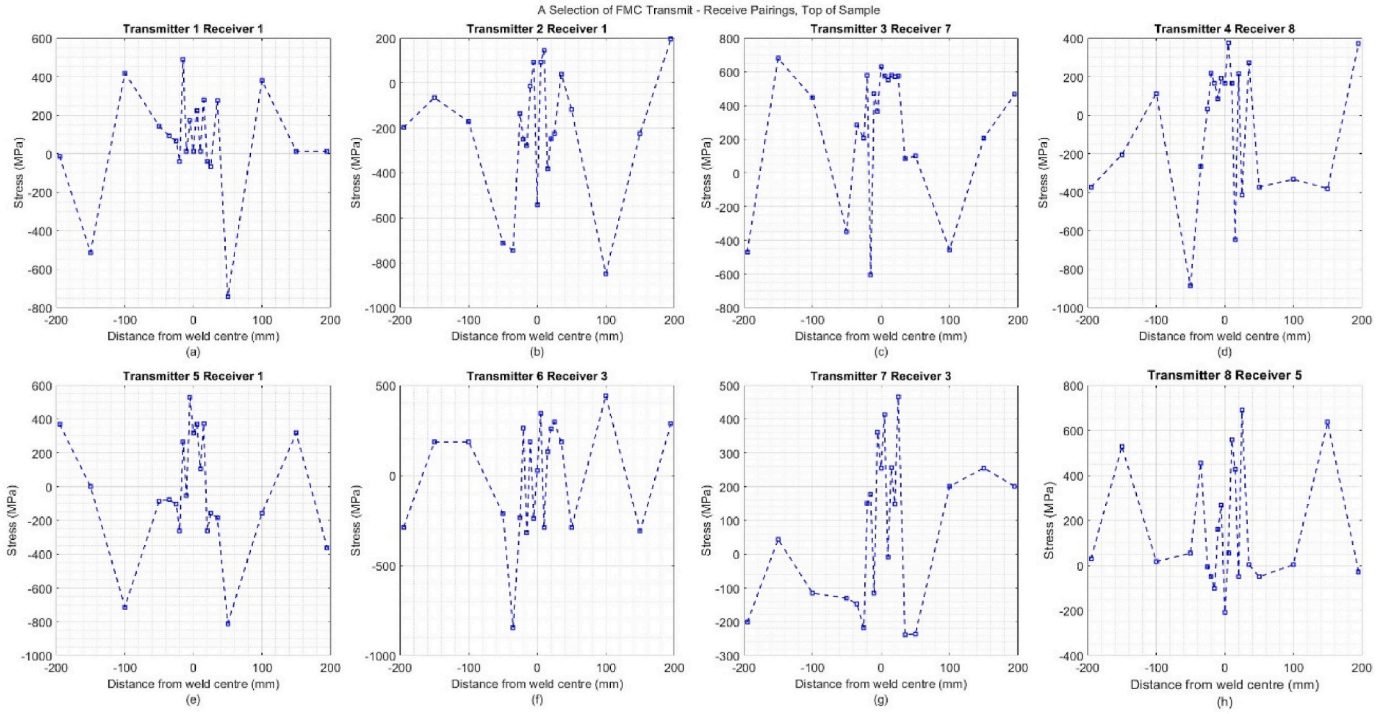

Fig. 20. A selection of the stress calculated across individual acoustic paths along the top of the weld sample.

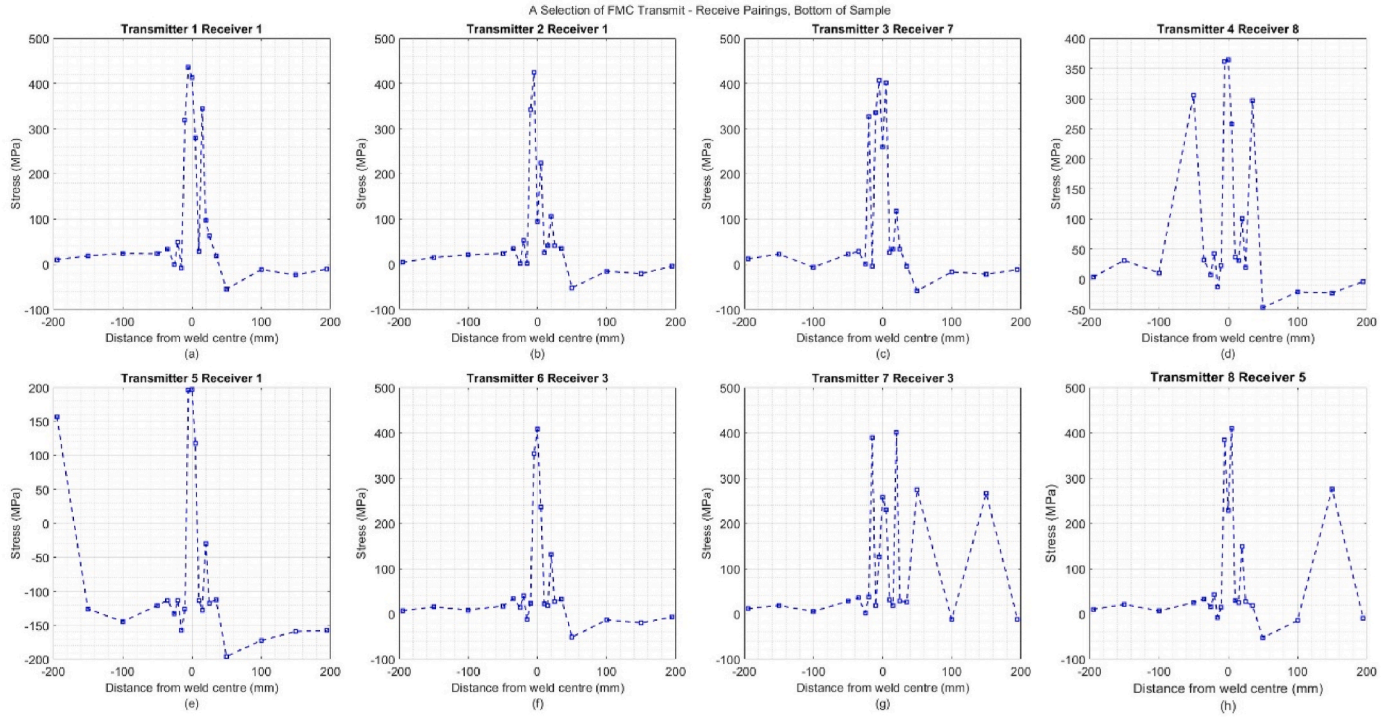

Fig. 21. A selection of the stress calculated across individual acoustic paths along the bottom of the weld sample.

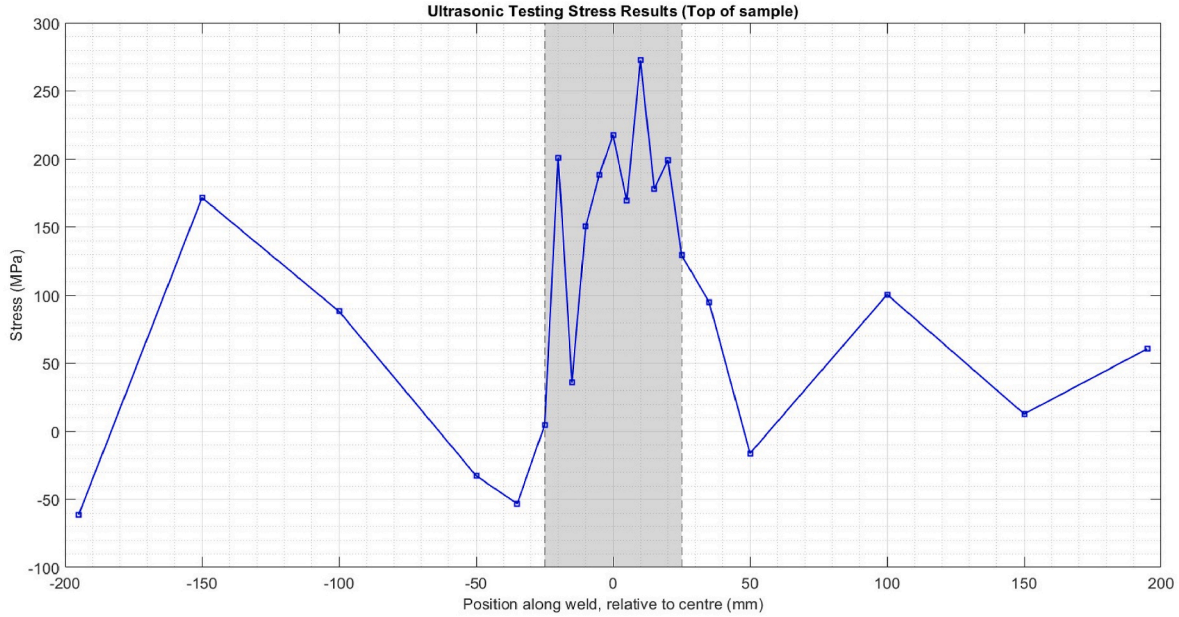

Fig. 22. Average RS across top of sample.

This component reflects stresses across the weld's width. While usually lower than longitudinal stress, it still provides critical information about the material's lateral integrity and response to welding-induced deformation.

3. Normal Stress (Perpendicular to the surface):

Measured through the sample's thickness, normal stress offers insights into through-thickness effects, which are especially important for assessing potential delamination or subsurface defects.

The ND results revealed distinct stress patterns consistent with expected RS distributions in welded structures: As anticipated, longitudinal stresses were significantly higher than transverse stresses. This aligns with the typical behaviour of welded joints, where longitudinal stresses develop due to thermal expansion along the weld axis and subsequent contraction upon cooling. Pronounced stress peaks were observed within the central region of the weld, specifically between −25 mm and 25 mm. This region corresponds to the weld cap, where the material experiences the most intense thermal cycles during welding. These stress concentrations are critical for assessing potential failure points, as high RS can lead to cracking or fatigue issues over time. Additional stress peaks were noted in the regions between −40 mm and

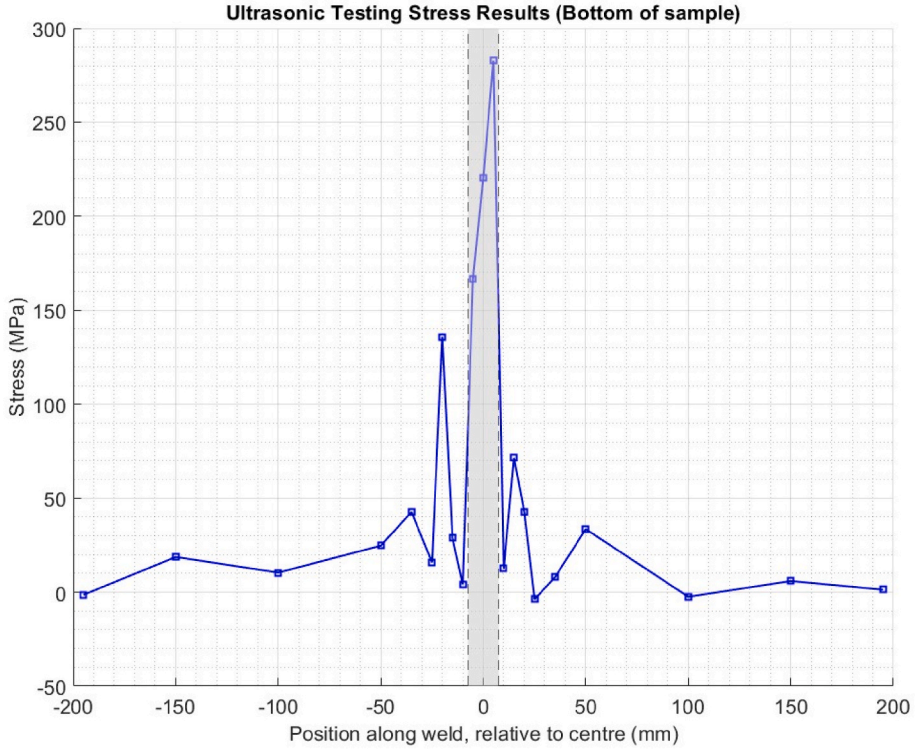

Fig. 23. Average RS across bottom of sample.

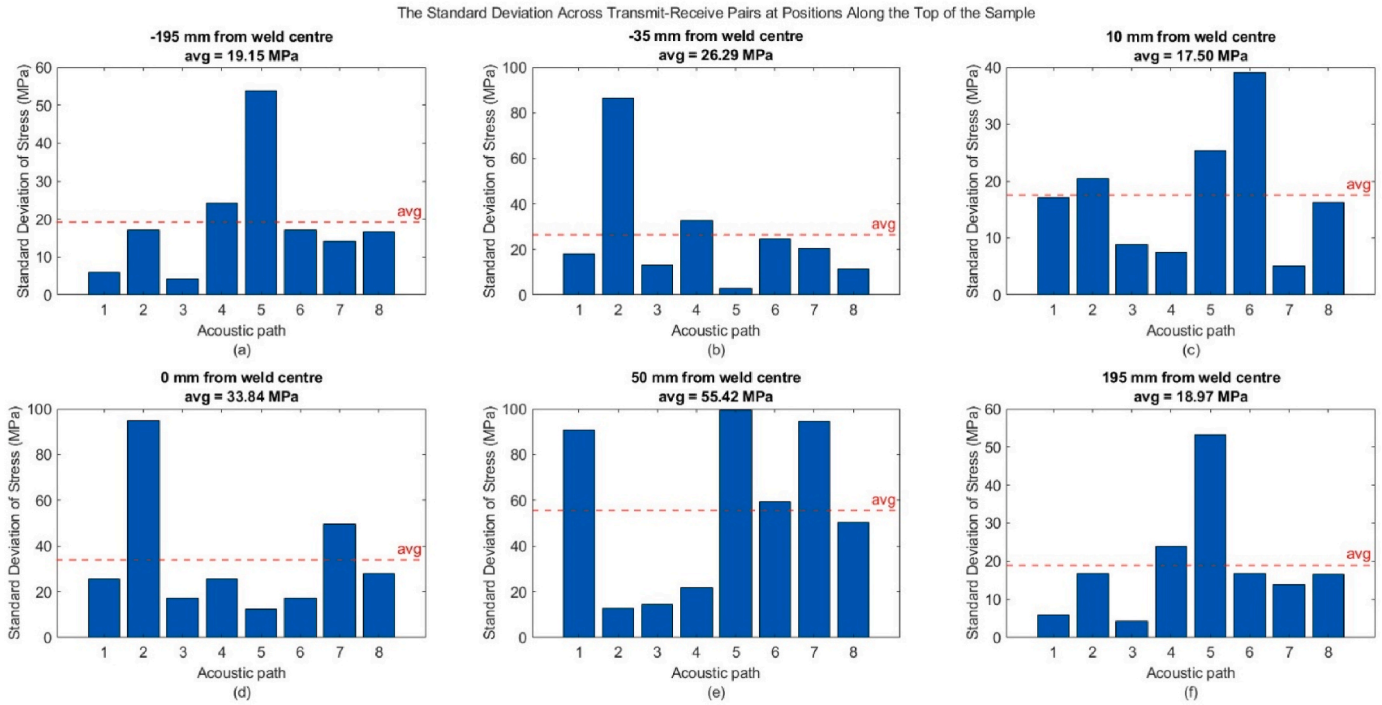

Fig. 24. A selection of standard deviation examples across matched transmit-receive pairs along the top of the weld sample. These are at positions relative to the weld centre: (a) −195 mm, (b) −35 mm, (c) 10 mm, (d) 0 mm, (e) 50 mm, and (f) 195 mm.

−25 mm and 25 mm–40 mm, which mark the boundaries of the Heat-Affected Zone (HAZ). The HAZ undergoes significant microstructural changes due to the heat input during welding, leading to RS accumulation. These sharp increases indicate the extent of thermal influence and provide essential data for evaluating the weld's mechanical performance. These results provide a reliable baseline for RS assessment, offering depth-resolved data that ultrasonic and IHD methods can be judged against. This thorough comparison ensures that any anomalies or discrepancies are identified and addressed, enhancing the overall confidence in the stress analysis. By combining ND, ultrasonic, and IHD data, a comprehensive understanding of the weld's RS state is achieved, facilitating better predictions of performance and potential failure

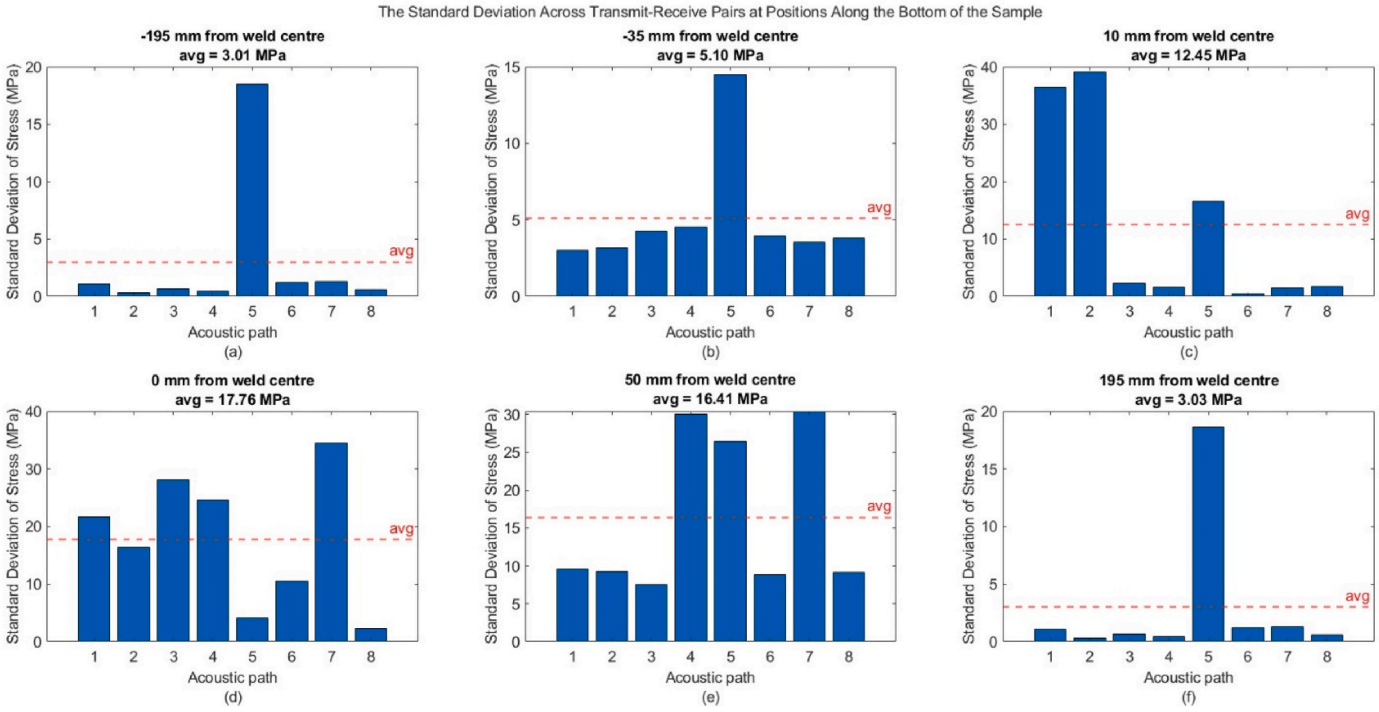

Fig. 25. A selection of standard deviation examples across matched transmit-receive pairs along the bottom of the weld sample. These are at positions relative to the weld centre: (a) −195 mm, (b) −35 mm, (c) 10 mm, (d) 0 mm, (e) 50 mm, and (f) 195 mm.

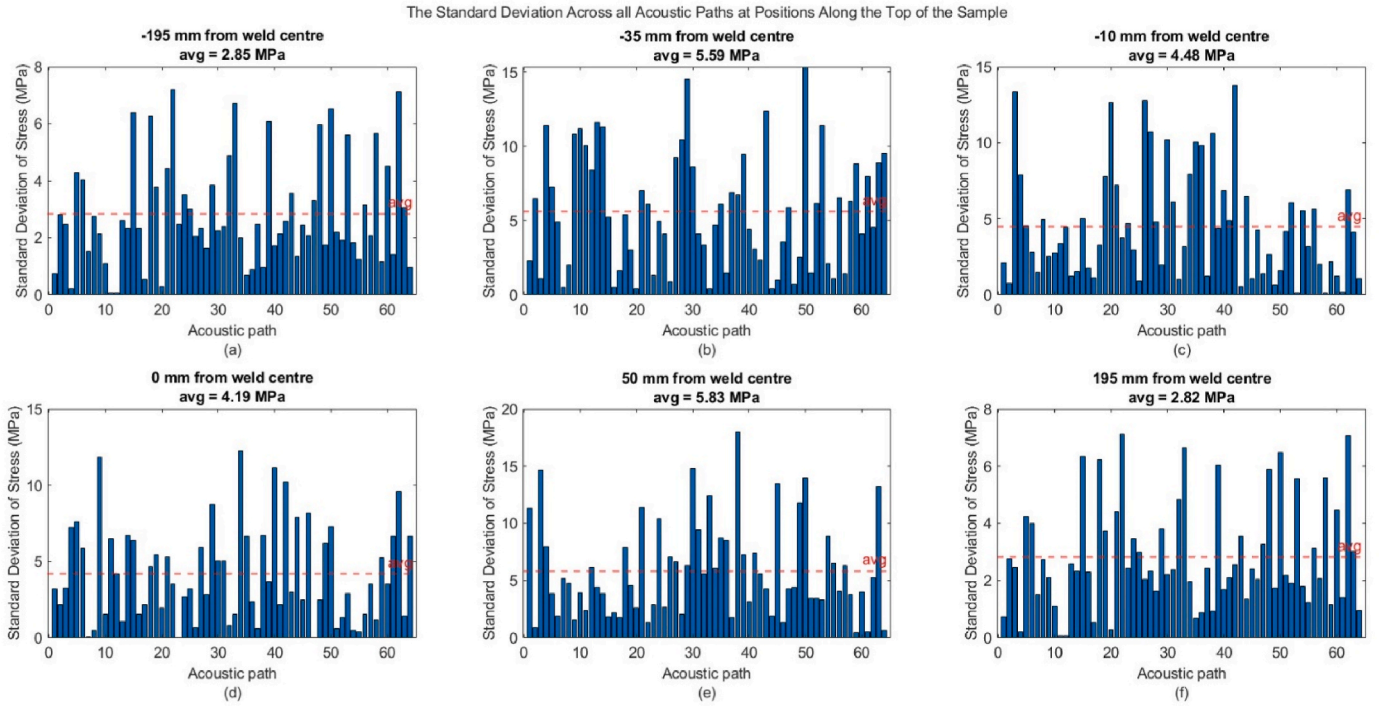

Fig. 26. A selection of standard deviation examples across matched all acoustic paths along the top of the weld sample. These are at positions relative to the weld centre: (a) −195 mm, (b) −35 mm, (c) 10 mm, (d) 0 mm, (e) 50 mm, and (f) 195 mm.

mechanisms.

4.4. Comparison

The results obtained from each technique were systematically overlaid to facilitate direct comparison (Figs. 29 and 30). This comprehensive evaluation offered a clear perspective on the performance of each method, revealing that while there is a strong quantitative alignment between them, qualitative discrepancies arise due to the unique advantages and constraints of each approach.

Focusing on the central region of the weld cap at the top of the sample, the ND method measured an RS value of 378.32 MPa. This is

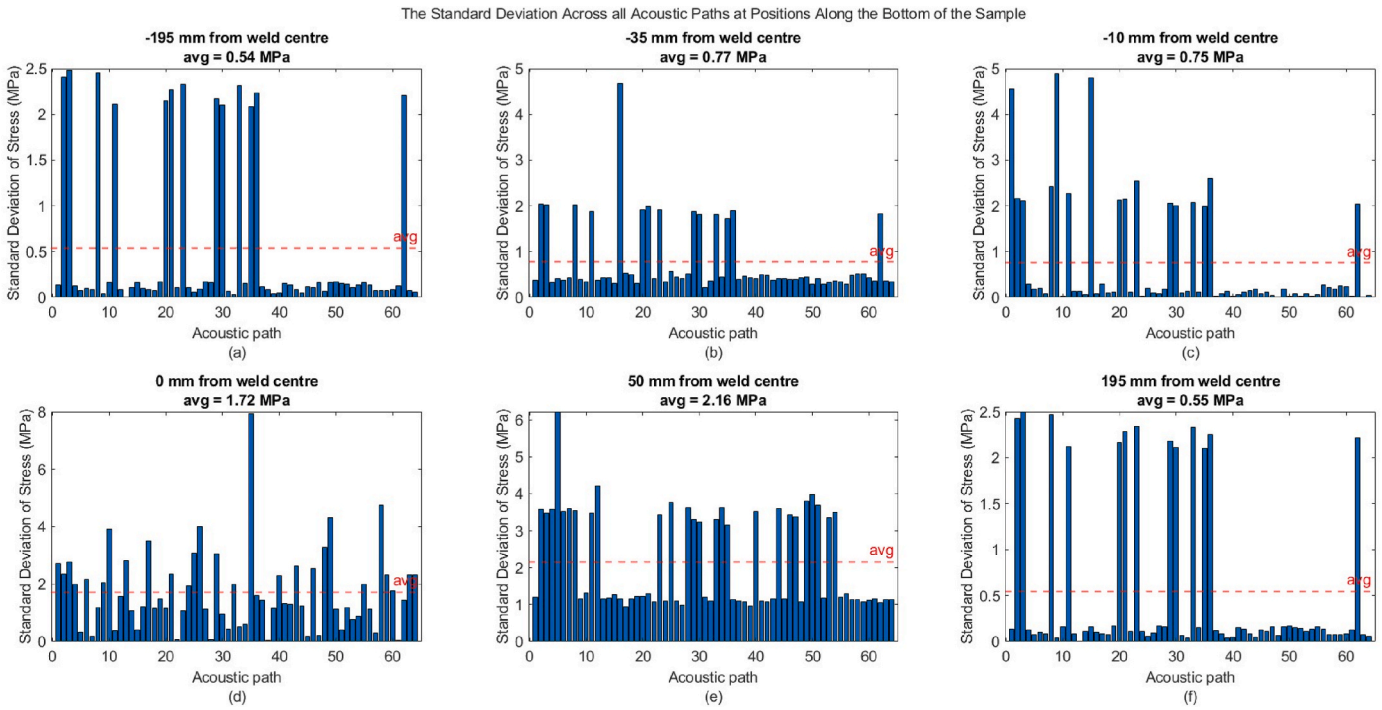

Fig. 27. A selection of standard deviation examples across matched all acoustic paths along the bottom of the weld sample. These are at positions relative to the weld centre: (a) −195 mm, (b) −35 mm, (c) 10 mm, (d) 0 mm, (e) 50 mm, and (f) 195 mm.

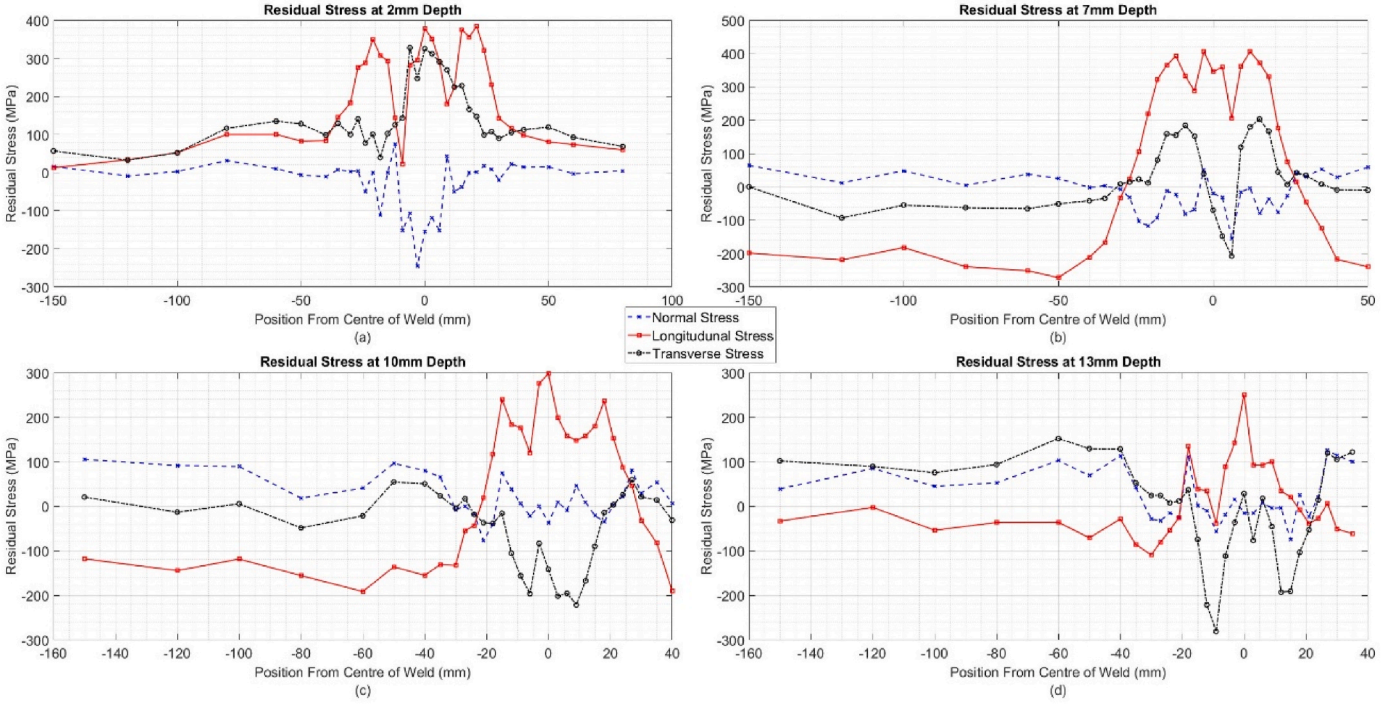

Fig. 28. Nd results with normal stress (blue), longitudinal stress (red), and transverse stress (black).

because overmatched welding was performed, that is the weld material has a higher yield stress than the parent material. This was anticipated due to the lack of tempering in the manufacturing process, and as similar trends have been reported in previous studies on two different grades of steel welds (low-carbon steel and high-strength low-alloy steel), where residual stresses were found to exceed the nominal yield strength of both the parent and weld metals by as much as 150 MPa [37,38]. Therefore, this value is considered a benchmark because of ND's non-contact measurement capability and its inherent depth-resolved precision, which minimises errors associated with surface irregularities. By contrast, the PAURS technique recorded a lower RS value of 217.82 MPa. This disparity can be attributed to the complex geometry of the sample in the weld cap and root, which induces irregularities in ultrasonic wave propagation and can significantly influence signal interpretation. The IHD method, finally, yielded an average RS value of 243 MPa across three measurement sites. While IHD's semi-destructive nature

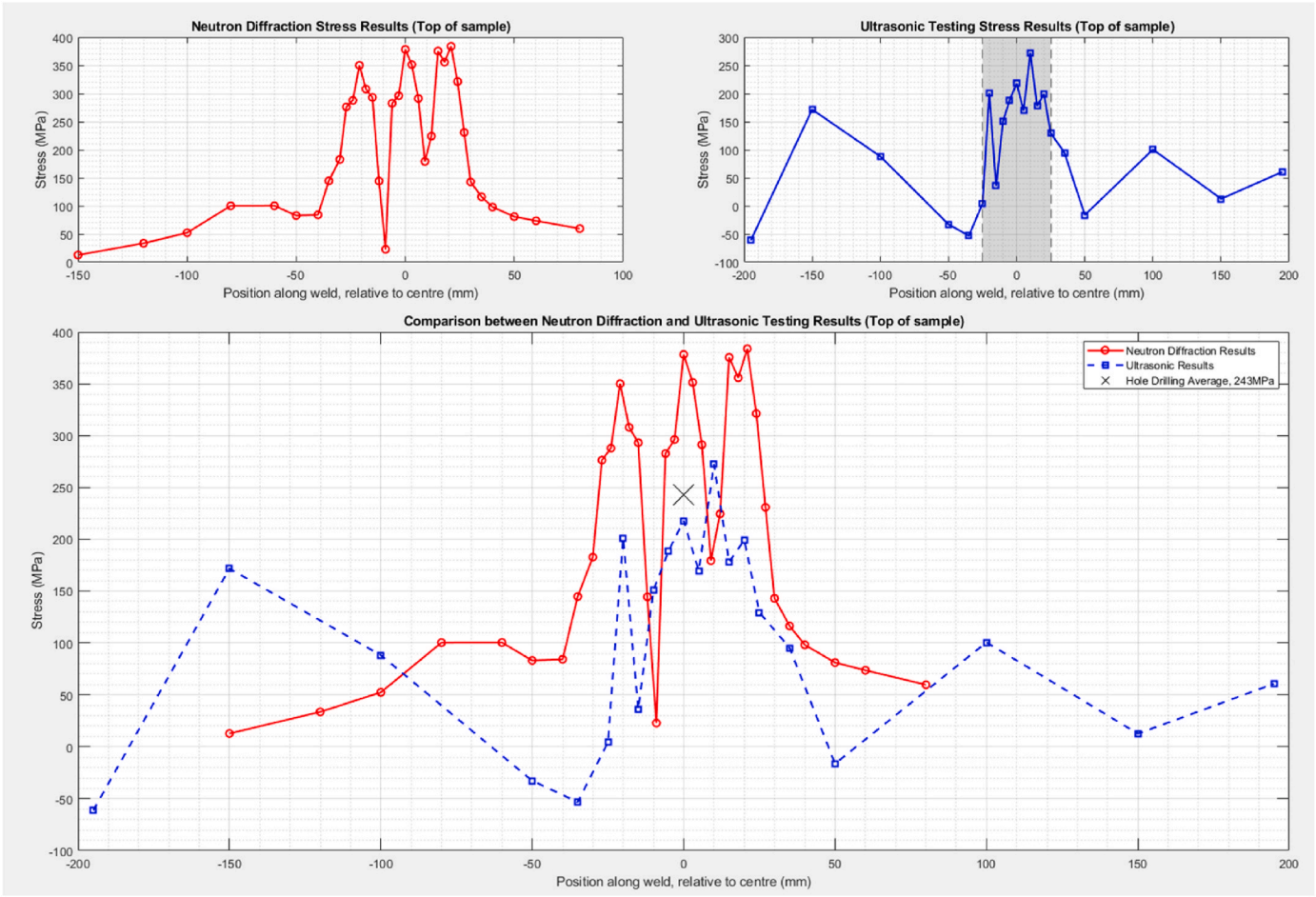

Fig. 29. Comparison between IHD, ND, and PAURS for the top surface of the welded plate.

provides a valuable means of cross-verification, its precision can decline in areas with shallow measurement depths or in regions characterised by complex material responses.

The average RS value calculated from all three methods at the weld centre was 279.71 MPa. This convergence suggests a reasonable level of agreement among the techniques, even though individual measurements exhibited some variability. These results underscore the capacity of the PAURS method to produce data that aligns closely with established approaches, demonstrating its potential as a reliable alternative despite its relative novelty. However, the results also highlight critical factors influencing measurement outcomes, particularly the weld geometry. The irregular weld cap at the top surface appears to be a significant contributor to the observed discrepancies. Ultrasonic waves are highly sensitive to surface irregularities, which can distort or reflect the signals, leading to less accurate measurements. In contrast, ND and IHD methods proved less vulnerable to these surface effects, providing more consistent results. Supporting this conclusion is the fact that measurements taken on the smoother bottom surface, near the weld root, exhibited closer agreement among the PAURS and ND techniques, with the results from the two methodologies fully overlapping in some areas. The reduced geometric complexity at the bottom minimised signal distortion, reinforcing the reliability of ultrasonic methods in simpler configurations.

Overall, these findings indicate that the PAURS method, though still in its early stages of development, demonstrates commendable quantitative alignment with well-established techniques. Nevertheless, areas for improvement have also been identified. Enhancing the capabilities of phased array ultrasonic probes presents an opportunity to address specific challenges associated with weld geometry. For instance, advanced signal processing techniques could be developed to mitigate the influence of irregular surfaces, and customised probe designs may improve adaptability to complex geometries.

Future research should prioritise solutions for inspecting intricate weld geometries more effectively. Potential directions include the development of correction algorithms capable of accounting for wave distortion and the integration of supplementary imaging techniques to enhance ultrasonic data interpretation. Moreover, the unique advantages of the PAURS method, such as its rapid scanning capabilities and the ability to focus on localised regions within a sample, could be leveraged more strategically. By addressing current limitations, these capabilities have the potential to significantly improve both the accuracy and reliability of the technique. This iterative refinement process will be critical in fully realising the potential of ultrasonic methods for assessing RS in complex welded structures.

5. Conclusions

This study combined robotic welding, finite element modelling of ultrasonic wave propagation, phased array ultrasonics, tensile testing for acoustoelastic coefficient measurement, Neutron Diffraction (ND), and Incremental Hole Drilling (IHD) methods for Residual Stress (RS) measurement to demonstrate the potential of Phased Array Ultrasonics for Residual Stress Measurement (PAURS) as a novel, non-destructive method for measuring RS in welded structures. The results from PAURS were compared with ND and IHD methods for validation.

- The IHD method, following ASTM E837 – 13a, was conducted at three positions on the weld sample, measuring RS at depths up to 1

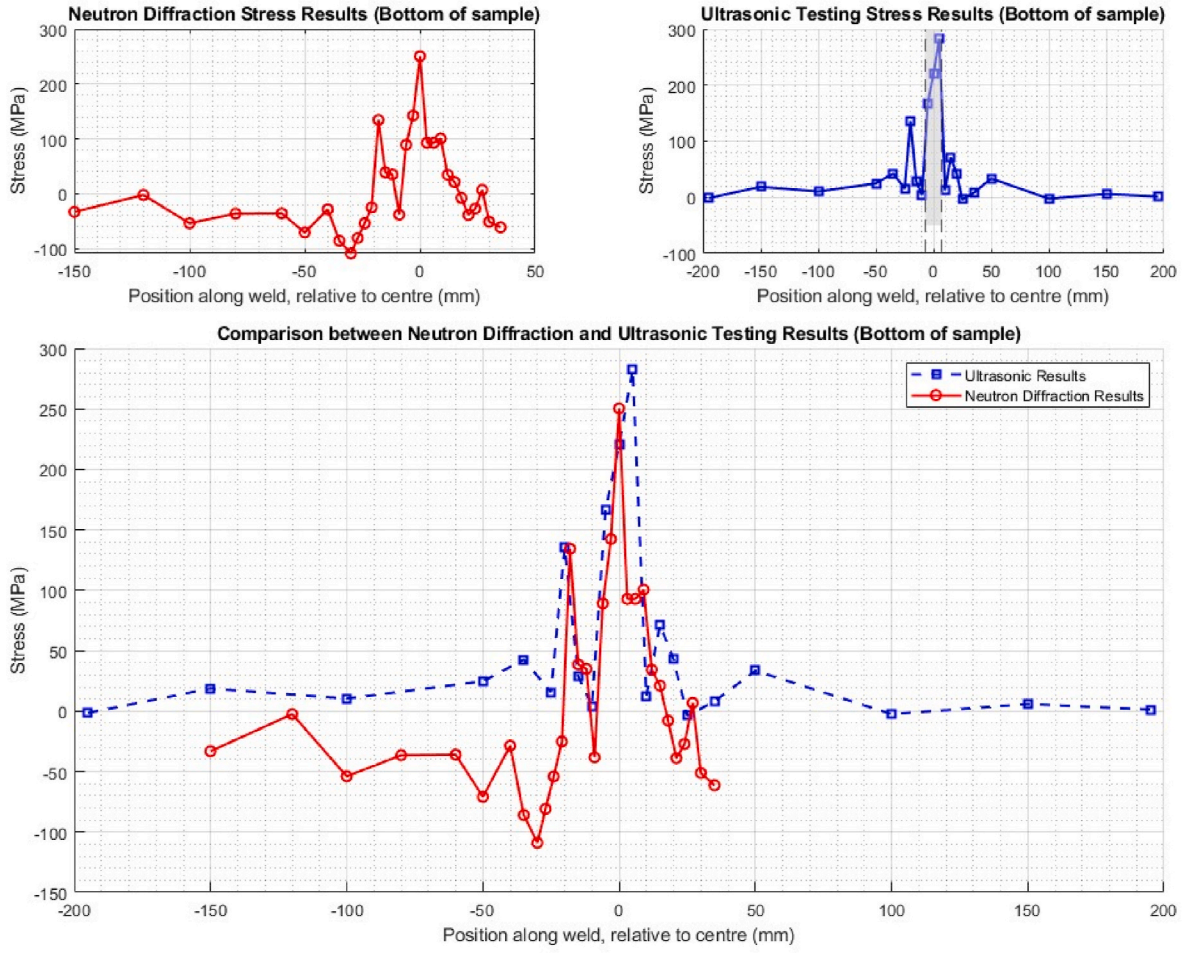

Fig. 30. Comparison between ND, and PAURS for the bottom surface of the welded plate.

mm. Strain gauges recorded data during IHD, correlating with the expected LCR wave penetration depth. This provided RS measurement results at the weld centre, ensuring reliable stress measurements in the 200–1000 μm depth range.

- Pogo finite element modelling successfully simulated LCR wave propagation, optimizing the wedge angle for PAURS, validating LCR wave characteristics, and demonstrating its potential for stress measurement and advancements in ultrasonic methods. Pogo simulations, wedge manufacturing, tensile testing, and ToF measurements using phased array ultrasonics were combined to complete the PAURS setup, generating comprehensive results for both top and bottom weld sample analyses. Discrepancy analysis showed that FMC significantly reduced the standard deviation in RS measurements, lowering inconsistencies by 5–10 times compared to linear paths, particularly enhancing accuracy in the HAZ and weld zone.
- The ND method provided the RS distribution in the weld sample, offering depth-resolved data (at 2 mm, 7 mm, 10 mm, and 13 mm depths) on longitudinal, transverse, and normal stresses, with pronounced peaks in the weld cap and HAZ regions, establishing a reliable baseline for evaluating PAURS method and enhancing the overall understanding of the weld's stress state.
- Based on a direct comparison of the IHD, ND, and PAURS methods, it can be concluded that the PAURS method showed strong qualitative alignment with established techniques, demonstrating its potential as a reliable alternative. Despite a lower peak RS value compared to ND in the weld centre during the top surface measurement, PAURS performed well in simpler configurations, especially on the smoother bottom surface, where its results aligned closely with ND. Its rapid scanning capabilities and ability to focus on localized regions, with a very competitive small measurement gauge, provide significant value to RS assessment.

PAURS has shown significant promise as a non-destructive method for assessing RS, particularly through its qualitative insights. With continued refinement, it has the potential to become a more reliable and widely adopted technique for RS measurement in complex welding scenarios.

CRediT authorship contribution statement

Brandon Mills: Writing – original draft, Visualization, Validation, Software, Methodology, Investigation, Formal analysis, Data curation. **Joseph Walker:** Writing – review & editing, Investigation. **Yashar Javadi:** Writing – review & editing, Supervision, Resources, Project administration, Investigation, Funding acquisition, Conceptualization. **Charles N. MacLeod:** Writing – review & editing, Supervision, Funding acquisition. **Houman Alipooramirabad:** Writing – review & editing, Validation, Methodology, Investigation, Formal analysis, Data curation. **Mark Reid:** Supervision, Project administration, Funding acquisition. **Anna Paradowska:** Supervision, Project administration, Investigation.

Declaration of competing interest

The authors declare that they have no known competing financial interests or personal relationships that could have appeared to influence the work reported in this paper.

Acknowledgements

This work was a multi-disciplinary collaboration between various organisations, each supporting different aspects of the project. The robotic welding and sensor development were undertaken as part of the EPSRC-supported UK Research Centre in NDE (RCNDE – EP/L022125/1). Neutron Diffraction (ND) was supported by a beam-time project from ANSTO (N:P15462). Incremental Hole Drilling (IHD) was performed at StressCraft Ltd. The authors would like to acknowledge EPSRC, RCNDE, and ANSTO for their support and funding of the projects. The authors would also like to acknowledge Dr. Phil Whitehead and StressCraft Ltd. for conducting the IHD measurements.

Data availability

Data will be made available on request.

References

[1] M.E. Fitzpatrick, A.T. Fry, P. Holdway, F.A. Kandil, J. Shackleton, L. Suominen, Determination of residual stresses by X-ray diffraction, Measurement Good Practice Guide 74 (2) (2005).
[2] A. Joseph, S. Rai, T. Jayakumar, N. Murugan, Evaluation of residual stresses in dissimilar weld joints, Int. J. Pres. Ves. Pip. 82 (2005) 700–705.
[3] G. Totten, M. Howes, T. Inoue, Handbook of Residual Stress and Deformation of Steel, ASM International, 2002.
[4] M. Prime, M. Hill, A. DeWald, R. Sebring, V. Dave, M. Cola, Residual stress mapping in welds using the contour method, in: *Trends In Welding Research, Proceedings Of the 6th International Conference*, Pine Mountain, 2002.
[5] N. Rossini, M. Dassisti, K. Benyounis, A. Olabi, Methods of measuring residual stresses in components, Mater. Des. 35 (2012) 572–588.
[6] H. Dai, J. Francis, H. Stone, H. Bhadehia, P. Withers, Characterising phase transformations and their effects on ferritic weld residual stresses with x-rays and neutrons, Metall. Mater. Trans. 39A (2008) 3070–3078.
[7] Y. Kurdryavtsev, J. Kleiman, Ultrasonic technique and equipment for residual stresses measurement, in: Engineering Applications of Residual Stress, Springer, 2011, pp. 55–56.
[8] American society for Testing and Materials, ASTM E837-20, Standard Test Method for Determining Residual Stresses by the Hole-Drilling Strain-Gage Method, ASTM International, West Conshohocken, PA, 2020.
[9] Y. Javadi, M. Akhlaghi, M. Najafabadi, Using finite element and ultrasonic method to evaluate welding longitudinal residual stress through the thickness in austenitic stainless steel plates, Mater. Des. 45 (2013) 628–642.
[10] M. Hutchings, P. Withers, T. Holden, T. Lorentzen, Fundamentals of neutron diffraction, in: Introduction to the Characterization of Residual Stress by Neutron Diffraction, CRC Press, 2005, pp. 25–67.
[11] G. Webster, R. Wimpory, Non-destructive measurement of residual stress by neutron diffraction, J. Mater. Process. Technol. 117 (2001) 395–399.
[12] M. Shokrieh, A.R.G. Mohammadi, Nondestructive testing (NDT) techniques in the measurement of residual stresses in composite materials: an overview, in: Residual Stresses in Composite Materials, Woodhead Publishing, 2021, pp. 71–109.
[13] M. Park, H. Yang, D. Jang, J. Kim, T. Jin, Residual stress measurement on welded specimen by neutron diffraction, J. Mater. Process. Technol. 155–156 (2004) 1171–1177.
[14] M. Mochizuki, M. Hayashi, T. Hattori, Measurement, numerical analysis of welding residual stress and its verification using neutron diffraction, J. Eng. Mater. Technol. 122 (1) (2000) 98–103.
[15] D.M. Egle, D.E. Bray, Measurement of acoustoelastic and third-order elastic constants for rail steel, J. Acoust. Soc. Am. 60 (1976) 741–744.
[16] Y. Hwang, G. Kim, Y. Kim, J. Park, M. Choi, K. Kim, Experimental measurement of residual stress distribution in rail specimens using ultrasonic LCR waves, Appl. Sci. 11 (2021) 9306.
[17] T. Salamnca, D. Bray, Residual stress measurement in steel plates and welds using critically refracted longitudinal (LCR) waves, Res. Nondestr. Eval. 7 (1996) 169–184.
[18] Y. Javadi, V. Plervis, M. Najafabadi, Using LCR ultrasonic method to evaluate residual stress in dissimilar welded pipes, International Journal of Innovation, Management, and Technology 4 (2013) 170–174.
[19] Y. Javadi, M. Vailev, R. Vithanage, A. Hutchison, R. Zimmerman, D. Lines, E. Mohseni, C. Macleod, G. Pierce, J. Menhen, A. Gachagan, Robotic residual stress measurement using phased array ultrasonic method, in: 59th Annual British Conference on Non-destructive Testing 2022, 2022. Telford.
[20] J. Walker, B. Mills, Y. Javadi, C. Macleod, Y. Sun, P.K. Taraphdar, B. Ahmad, S. Gurumurthy, J. Ding, F. Sellars, Study of residual stress using phased array ultrasonics in Ti-6AL-4V wire-arc additively manufactured components, Sensors 24 (19) (2024).
[21] Y. Javadi, H. Sergej, Employing the LCR waves to measure longitudinal residual stresses in different depths of a stainless steel welded plate, Adv. Mater. Sci. Eng. (2013).
[22] P. Huthwaite, "Pogo ultrasonic simulation software," Imperial College, [Online]. Available: http://www.pogo.software/. [Accessed 14 February 2025].
[23] Z. Abiza, M. Destrade, R. Ogden, Large acoustoelastic effect, Wave Motion 49 (2) (2012) 364–374.
[24] L. Landau, E. Lifshitz, Theory of Elasticity, 1989.
[25] M. Mohammadi, J.J. Fesharaki, Determination of acoustoelastic/acoustoplastic constants to measure stress in elastic/plastic limits by using LCR wave, NDT E Int. 104 (2019) 69–76.
[26] Y. Javadi, H.S. Pirzaman, M.H. Raeisi, M.A. Najafabadi, Ultrasonic inspection of a welded stainless steel pipe to evaluate residual stresses through thickness, Mater. Des. 49 (2013) 591–601.
[27] H. Alipooramirabad, S. Kianfar, A. Paradowska, R. Ghomashchi, Residual stress measurement in engine block—an overview, Int. J. Adv. Des. Manuf. Technol. 131 (1) (2024) 1–27.
[28] H. Alipooramirabad, A. Paradowska, O. Lavigne, R. Ghomashchi, M. Reid, In situ neutron diffraction measurement of strain relaxation in welds during heat treatment, Sci. Technol. Weld. Join. 22 (6) (2017) 484–495.
[29] KUKA, KUKA Robot Programming 1, Augsburg: KUKA Roboter GmbH, 2015.
[30] J. Guo, H. Fu, B. Pan, R. Kang, Recent progress of residual stress measurement methods: a review, Chin. J. Aeronaut. 34 (2) (2021) 54–78.
[31] P. Huthwaite, Accelerated finite element elastodynamic simulations using the GPU, J. Comput. Phys. 257 (2014) 687–707.
[32] G. West, S. Haslinger, J. Bamber, M. Lowe, P. Huthwaite, E. Harris, Simulation of ultrasound backscatter coefficient measurement using the finite element method, Ultrasonics 143 (2024).
[33] G. Sarris, S. Haslinger, P. Huthwaite, P. Nagy, M. Lowe, Attenuation of Rayleigh waves due to three-dimensional surface roughness: a comprehensive numerical evaluation, J. Acoust. Soc. Am. 154 (2) (2023) 808–818.
[34] D. Bray, Current Directions of Ultrasonic Stress Measurement Techniques, NDT.net, 2000 [Online]. Available: https://www.ndt.net/article/wcndt00/papers/idn647/idn647.htm. (Accessed 5 December 2024).
[35] D. Bray, W. Tang, Evaluating stress gradients in steel plates and bars with the LCR ultrasonic wave, in: ASME Pressure Vessels and Piping Conference, 1997. Orlando.
[36] Y. Javadi, S.H. Mosteshary, Evaluation of sub-surface residual stress by ultrasonic method and finite-element analysis of welding process in a monel pressure vessel, J. Test. Eval. 45 (2) (2017).
[37] J. Price, A. Paradowska, S. Joshi, T. Finlayson, Residual stresses measurement by neutron diffraction and theoretical estimation in a single weld bead, Int. J. Pres. Ves. Pip. 83 (5) (2006) 381–387.
[38] H. Alipooramirabad, A. Paradowska, R. Ghomashchi, A. Kotousov, M. Reid, Quantification of residual stresses in multi-pass welds using neutron diffraction, J. Mater. Process. Technol. 226 (2015) 40–49.